Aus dem
Institut für Neuropathologie
Institut der Ludwig-Maximilians-Universität München

Assessment of cytotoxicity against diffuse midline gli drug-induced neurotoxicity of novel chemotherapeuti

Dissertation
zum Erwerb des Doktorgrades der Medizin
an der Medizinischen Fakultät der
Ludwig-Maximilians-Universität zu München

vorgelegt von
Kaltra Begaj

aus
Fier, Albanien

Jahr
2024

Mit Genehmigung der Medizinischen Fakultät der
Ludwig-Maximilians-Universität München

Erstes Gutachten:	Prof. Dr. Jochen Herms
Zweites Gutachten:	Prof. Dr. Niklas Thon
Drittes Gutachten:	Prof. Dr. Maximilian Niyazi

Dekan:	Prof. Dr. med. Thomas Gudermann

Tag der mündlichen Prüfung: 11.01.2024

Acknowledgments

I am truly grateful to my supervisor Prof. Dr. med. Jochen Herms, as without his continuous support and invaluable feedback, this thesis would not have been possible.

I would like to equally express my deep appreciation to Dr. med Alexander Beck for his dedicated guidance, support, and invaluable patience during the running of this project. It was his enthusiasm and determination in the field of paediatric neuro-oncology, that motivated me to pursue research in this area.

I also could not have undertaken this journey without the support of my doctoral committee, Prof. Dr. med. Niklas Thon and Prof. Dr. med. Jörg-Christian Tonn, who provided me with thoughtful feedback on this dissertation.

Furthermore, I would like to thank the rest of the research team, Marbod Klenner, Christina Schmidt, Pia Freidel and Ph.D. Nicholas J.A. Tokarew for their constructive suggestions, which were very influential in the data-collection.

I would like to thank my colleagues and friends in the Institute for Neuropathology and Prion research – Ph.D. Dr. med. Mario M. Dorostkar, Dipl. -Ing. Peer Schmitz and Ph.D. Jeannine Widmann, for a cherished time spent together and for always boosting my morale.

I am deeply grateful to my partner, Robert Calaminus, for his unbelievable support and understanding during the preparation of this dissertation. My very special thanks, go also to my mother and my sister, Edlira Tahiraj and Uarda Begaj, who are my number one fans and to whom I dedicate this thesis.

Abstract:

Central nervous system (CNS) tumors are the second most common pediatric malignancy in Germany after leukaemia and the leading cause of cancer-related death in childhood. Diffuse midline glioma (DMG) is a highly malignant glioma that accounts for only 15-20% of all CNS tumors in children, yet is responsible for the highest mortality rate in this patient population.

The poor prognosis of 9-15 months after diagnosis and the only marginal survival benefits of current treatment options highlight the need for new therapeutic approaches.

The aim of this thesis is to identify promising novel therapies against DMG using robust, preclinical, animal-free cell models to provide a basis for planning clinical trials.

A single-agent sensitivity drug screen against DMG and a neurotoxicity assessment of thirty novel chemotherapeutic agents identified HSP90 inhibitors HSP990 and SNX2112 and NAMPT inhibitor daporinad as promising anti-DMG candidates with a wide therapeutic window.

In this thesis, no animal-based experiments were conducted, as they are not only time-consuming, ethically controversial, and expensive, but also have limited translatability to humans. Five patient-derived DMG cell lines were used for sensitivity drug screening, whereas neurons for neurotoxicity screening were differentiated from human pluripotent cells. By using customized patient-specific tumor cells and iPSCs, it is possible to develop personalized therapies for patients using the same methods as in this work.

Our in vitro drug screening provides insights into neurotoxicity and efficacy against various DMG cell lines but does not account for other treatment challenges such as BBB penetration, drug resistance, and cell-environment interaction. Given the complexity of treating DMG, further, more in-depth drug validation experiments are needed.

Zusammenfassung:

Tumore des zentralen Nervensystems (ZNS) sind nach Leukämien die zweithäufigste pädiatrische Tumorerkrankung in Deutschland und die führende Ursache für krebsbedingte Todesfälle im Kindesalter. Diffuse Mittelliniengliome (DMG) sind hochmaligne pädiatrische ZNS-Tumore, die zwar nur 15-20 % aller Hirntumoren im Kindesalter ausmachen aber für die höchste Mortalität in dieser Patientengruppe verantwortlich sind.

Die ungünstige Prognose der DMG mit einem Gesamtüberleben von 9 - 15 Monate nach Diagnosestellung und die bis dato nur marginalen Überlebensvorteile der bisherigen Behandlungsmöglichkeiten verdeutlichen den Bedarf an neuen therapeutischen Ansätzen.

Das Ziel dieser Arbeit ist es, durch den Einsatz robuster präklinischer tierfreier Zellmodelle neue therapeutische Optionen gegen DMG zu identifizieren und eine Grundlage für die Planung klinischer Studien zu bieten.

Durch ein in vitro Screening der zytotoxischen Wirkung von dreißig Chemotherapeutika gegen DMG-Tumorzellen und gesundes Nervengewebe konnten wir die HSP90-Inhibitoren HSP990 und SNX2112 sowie den NAMPT-Inhibitor Daporinad als vielversprechende Kandidaten mit einem breiten therapeutischen Fenster identifizieren.

In dieser Arbeit wurden keine tiergestützten Experimente durchgeführt, da sie nicht nur zeitaufwändig, ethisch umstritten und teuer sind, sondern die auch nur begrenzt auf den Menschen übertragbar sind. Für das Zytotoxizität-Screening gegen DMG-Tumorzellen wurden die Zellen von fünf DMG-Patienten gewonnen, während die Neuronen für das Neurotoxizitäts-Screening aus humanen pluripotenten Zellen differenziert wurden. Durch Verwendung von patientenspezifischen Tumorzellen und iPSCs ist es möglich mit denselben Methoden wie in dieser Arbeit personalisierte Therapien für Patienten zu entwickeln.

In Anbetracht der Herausforderungen bei der Behandlung von DMG, wie der Blut-Hirn-Schranke, der Entwicklung von Arzneimittelresistenzen oder der Mikroumgebung des Tumors, sind weitere, tiefergehende Experimente zur Arzneimittelvalidierung erforderlich.

Affidavit

Begaj, Kaltra

Surname, first name

I hereby declare, that the submitted thesis entitled

"Assessment of cytotoxicity against diffuse midline glioma and drug-induced neurotoxicity of novel chemotherapeutic agents"

is my own work. I have only used the sources indicated and have not made unauthorised use of services of a third party. Where the work of others has been quoted or reproduced, the source is always given.

I further declare that the dissertation presented here has not been submitted in the same or similar form to any other institution for the purpose of obtaining an academic degree.

Munich, 15.11.2024

Place, Date

Kaltra Begaj

Signature doctoral candidate

Table of Contents

List of abbreviations

The following list describes the meaning of various abbreviations and acronyms used throughout the thesis. The page on which each one is defined or first used is also given.

1. Introduction

1.1 **Diffuse midline glioma**

1.1.1 **Background**

Central nervous system (CNS) tumors are the second most common pediatric malignancy after leukaemia and the leading cause of cancer - related death in childhood (1, 2). Diffuse midline gliomas (DMG) account for 15 –20% of all CNS tumors in children. They contribute significantly to tumor-related mortality in this population by being the leading cause of death in children with brain tumors (3).

DMG is a highly malignant glioma (HGG) occurring almost exclusively in children with a mean overall survival (OS) of 9 - 15 months after diagnosis (4). This tumor entity has been recently redefined by the World Health Organization (WHO-2021) and includes malignancies previously referred to as diffuse intrinsic pontine glioma (DIPG) (5).

On the molecular level diffuse midline glioma is H3K27M-mutant with alterations in one of the two main histone variants, H3.3 or, less frequently, H3.1, encoded by the genes H3F3A and HIST1H3B respectively (6, 7). Phenotypically, the tumor is characterized by a diffuse growth pattern, and a midline location (e.g. thalamus, brain stem, and spinal cord) and accounts for 80% of all pediatric brain stem tumors (3, 5). The histological phenotype of the tumor varies widely and shares features with its adult counterparts, anaplastic astrocytoma (WHO grade III) or glioblastoma (GBM) (WHO grade IV) (5, 8).

1.1.2 **Diagnostics**

The clinical presentation and the characteristic magnet resonance (MR) findings are decisive for the diagnosis of DMG, while the histological and molecular characterization of the tumor still play a subordinate role in many countries (9, 10).
The neuropathological diagnosis of the tumor has changed over the past 20 years. Histological grading has altered neither the therapy nor the outcome of the patients, so that routine biopsy was discontinued as the standard of care in many countries in the early 1990s and MRI was introduced as a standard diagnostic

method (11, 12). As a result, these tumors were rarely biopsied, making their true incidence difficult to assess from cancer registry datasets and limiting the availability of tumor tissue for molecular studies (3, 13, 14). This approach has prevailed until recently. The safety of biopsy through minimally invasive techniques, greater knowledge of the tumor biology, and improved clinical trials when characterizing the tumor, make biopsy a low-risk asset in the diagnostic and investigation of novel therapies for diffuse midline glioma (15).

1.1.3 **Diagnostic considerations**

Differentiating between diseases with similar clinical presentation and overlap in imaging features through further appropriate diagnostic is fundamental and it further accentuates the diagnostic utility of biopsy. Tumorous lesions including low-grade gliomas (LGG), astrocytoma, glioblastoma and primitive neuroectodermal tumors of the central nervous system (CNS-PNET); and non-tumorous lesions including vascular malformations, cysts, demyelinating diseases, and inflammatory/infectious processes should be considered in the differential diagnosis of diffuse midline glioma (8, 16-18).

1.1.4 **Clinical presentation**

Diffuse midline glioma progresses rapidly, resulting in children typically having symptoms for a month or less before they are diagnosed (14). Affected patients may present a variety of neurological symptoms depending on the anatomical location of the lesion (8). The compression or infiltration of structures on and near the ventral pons, where the tumor typically originates, leads to one or more cranial nerve (CN) deficits (diplopia and facial asymmetry), pyramidal tracts signs (hyperrefflexia, upward Babinski, and extremity weakness) or cerebellar signs (ataxia, dysmetria, and dysarthria) (14, 19, 20). Together, these three frequently occurring neurological symptoms are referred to as the “classic triad” of diffuse midline glioma presentation and must always be clarified through proper diagnostics (8). Nonetheless half of patients may not demonstrate such typical findings, making diffuse midline glioma difficult to diagnose (9). Abducens palsy (cranial nerve VI), which usually manifests as dysconjugate gaze and horizontal uncrossed diplopia, is a highly sensitive clinical prodromal feature of diffuse midline

glioma, that can arouse suspicion of this diagnosis (20). Signs of increased intracranial pressure are not typical and only present in less than 10% of patients at the time of diagnosis. This symptom is caused by the dorsal tumor expansion and the resulting obstructive hydrocephalus and is more likely to occur in the end-stage of the disease (9, 21).

1.1.5 **Magnet resonance imaging features**

Some classical MR imaging features are a poorly circumscribed abnormal T2-elongation that typically involves more than 50% of the pons and a diffusely-enlarged, gadolinium-nonenhancing pontine mass, that commonly engulfs the basilary artery (10). These imagining features reflect the diffuse infiltrative nature of the tumor, intermixing with healthy tissue, and distinguish diffuse midline glioma from the less aggressive focal brainstem neoplasms (14).

Further MR imaging features of diffuse midline gliomas can be heterogeneous. Hemorrhage, necrosis, and visible diffusion restriction are frequently present features of the tumor, and their presentation alone should not preclude the diagnosis of diffuse midline glioma (22). In addition, some radiological features were observed more frequently depending on the anatomical location of the tumor (23, 24). A previous study demonstrated that diffuse midline gliomas located in the cervical spine are more likely to show cerebrospinal fluid (CSF)-based metastatic spread and tend to have a uniform enhancing (23). Thalamic and pontine gliomas are more likely to show a variety of progressive patterns, most commonly local recurrence, demonstrate contrast enhancement to a variable degree and are more likely to be solid or infiltrative and have infrequent necrosis (23).

MR imaging not only plays an essential role in diagnosing diffuse midline gliomas but can also be useful in assessing the response of diffuse midline gliomas to therapy and predicting patient survival (25, 26). Extrapontine extension, greater size, enhancement, necrosis, diffusion restriction, and distant metastases are significantly correlated with a poorer prognosis (22). Furthermore, a recent, retrospective study indicated that MR image texture analysis (MRTA) has a predictive value regarding the survival of patients with diffuse midline gliomas of the pons

and that homogenous tumor texture is significantly associated with poorer overall survival (26).

The World Health Organization Classification of Tumors of the Central Nervous System (WHO-2016) defines diffuse midline glioma as a new tumor entity based on its genetic alterations in H3K27M in addition to histopathologic and phenotypic features (5). Studies have been conducted to determine radiological distinctive features between H3K27M-mutant and wild type (WT) diffuse glioma tumors, that will allow a non-invasive distinction without the need for biopsy (23, 24).
An overlap of MR imaging features has been observed for the H3K27M-mutant and the wild type diffuse midline glioma when investigating characteristics such as size, contrast enhancement pattern, edema, radiomics properties, infiltrative patterns and T1WI, T2WI, and CeT1WI features (23, 24). Only the cystic formation demonstrated significant differences between mutant and WT diffuse glioma and may be useful for differentiating between these two groups (24).

A few other studies have evaluated distinctive features of diffuse midline glioma with histone mutation in H3.3 vs in H3.1. Studies found more necrosis, edema, ring enhancement and more restricted diffusion in H3.1 vs. H3.3 mutant tumors, but the correlations lack in strength and significance. (22, 27).

The poor correlation between imaging features and histone mutation status (H3 vs. WT or H3.3 vs. H3.1) makes a clinical differentiation of the different histone status based solely on the image features insufficient and underlines the importance of the biopsy for tumor characterization and the need for more advanced radiological approaches (22).

1.1.6 **Histopathological features**

The histological phenotype of diffuse midline glioma varies widely and shares features with its adult counterparts, anaplastic astrocytoma (WHO-grade III) or glioblastoma multiforme (WHO-grade IV). Less commonly, lesions exhibit characteristic features of a well-differentiated astrocytoma (WHO-grade II). (5, 8, 11, 21).

Increased mitotic activity, microvascular proliferation, and/or necrosis are present in most cases (8). Nonetheless, as mentioned, a fraction of cases shows lower grade histology, with an overall bland cytology and absence of the traditional high-grade features (8). Interestingly all lesions behave equally aggressively, despite the histological grading, underlining the significance of additional integration of molecular features (11).

Diffuse midline glioma stains positive for glioma-typical immunohistochemistry markers such as GFAP, ATRX, p53, neurofilament and ki-67. H3K27M-positive staining is characteristic for the tumor. Meanwhile BRAFV600E and IDH1 stains are typically negative (8).

1.1.1 **Molecular features**

Studies using various molecular approaches have identified a heterozygous missense mutation in the genes H3F3A or, less frequently, in HIST1H3B, encoding histone protein H3.3 and H3.1, respectively (6, 7, 27). The mutation results in the substitution of lysine for methionine at amino acid 27 (K27M) in one of the H3.1 or H3.3 isoforms, leading to an nearly global loss of histone trimethylation that ultimately induces epigenetic silencing (6, 8). Paradoxically, in addition to the loss of trimethylation, a dramatic increase in methylation at specific gene loci has also been described, particularly at promoters that alter the expression of genes implicated in various cancer pathways (28, 29).

Substitution of methionine for K27 also impairs the ability to acetylate at this site, with acetylated K27 associated with upregulation of genes (6). In addition to the extensive epigenetic regulation described above, H3 histone could potentially play a role in selective regulation of developmental genes and telomere length or stability (6).

Since alterations in H3K27M appear to be one of the founding event in diffuse midline glioma oncogenesis, they have been included by the World Health Organization (WHO-2016) as a criterion for defining the tumor (5, 27). Compared with wild-type cases, H3K27M-mutated tumors are associated with significantly worse outcomes, regardless of the isoform involved.

Tumours harbouring a K27M mutation in HIST1H3B (H3.1) are associated with less aggressive behaviour, fewer metastases and better response to

radiotherapy than their H3F3A (H3.3) counterpart. This discrepances in the tumor behavior suggests, that mutation in H3.3 and H3.1 drive two separate oncogenic programmes with potentialy distinct therapeutic targets (27).
Studies pointed out frequent up-regulation of receptor tyrosine kinases (RTKs) involved in RTK-RAS-PI3K-Akt signaling pathway, suggesting that targeted inhibition of RTKs may be useful in the therapy for diffuse midline glioma. In particular PDGFR-alpha, MET, IGF1R, PIK3R1 and PIK3CA are implicated (7, 30-33). Interestingly, PDGFA gain or amplification exclusively co-occur with H3F3A mutation, suggesting that it is a subsequent alteration or together with H3F3A (H3.3) co-segregated and is associated with an aggressive tumor behavior (7, 8). TP53 mutation is another alteration commonly present in conjunction with PDGFRA gain or amplification and is present in approximately 40% of diffuse midline glioma cases (8, 33).
Furthermore low level gains in Poly (ADP-ribose) polymerase (PARP) have been identified in some tumor cases, suggesting PARP inhibitions as a promising novel therapeutic target for some pediatric DIPGs (34).
Lastly, clonal missense in the ACVR gene has been observed exclusively in H3.1-mutant diffuse midline glioma and is associated with a younger patient age and a better overall survival (35). Additionally MYC/PVT1 amplification, SETD2 alterations and loss-of-function mutations in ATRX are also frequently present (7, 35). Detecting and better understanding driving mutations in diffuse midline glioma could lead to promising targeted therapies.

1.1.8 **Tumor metastasis**

Diffuse midline gliomas rarely metastasize beyond the central nervous system but can spread along fiber tracts to other areas of the brain or spinal cord. (9). Due to the infiltrative and diffuse growth pattern of the tumor, particularly nearby structures such as cerebellum and thalamus are invaded by the tumor, while distant sites of the CNS are rarely affected (8). Metastases within the neuraxis have been reported in 5-30% of patients in the course of their disease (36). The prognosis for affected patients remains dismal regardless of the presence of metas-

tases, since local failure in the primary site is the leading cause of death in patients with diffuse midline glioma (36, 37). Nevertheless, metastases can affect the quality of life as they may cause symptoms such as neck pain, lower limb weakness and hydrocephalus (36). In addition, metastases are of interest for possible future curative treatments of diffuse midline glioma.

1.1.9 Current treatment and prognosis

To date, the standard treatment remains fractionated, focal, intensity-modulated radiation therapy (IMRT) with a total radiation dose of 54–60 Gy, spread over a period of 6 weeks (38). Due to the eloquent location and infiltrative nature of the tumor, diffuse midline glioma is not surgically resectable (39). Furthermore, many chemotherapy regimens have so far not provided significant benefit (8).
Despite numerous clinical studies, the prognosis of affected children has hardly changed in the past three decades (3). Diffuse midline glioma is almost inevitably fatal with a mean OS of 8–14 months from the time of diagnosis (38). Radiation therapy leads to transient improvements and extends the progression-free survival by an average of 3 to 6 months but is still viewed as an aggressive palliative therapy (38, 39). This insufficient treatment emphasizes the need for novel therapeutic strategies.

1.1.10 Novel therapeutic strategies

Several potential therapeutic approaches for DMG are currently in pre-clinical or clinical investigation. These include among others epigenetic targeted therapies, growth factor targeted therapies and immunotherapy.

1.1.10.1 Epigenetic targeted therapies

A better understanding of the H3K27M mutation and subsequent loss of histone trimethylation and acetylation as driving events in diffuse midline glioma oncogenesis gives rise to promising targeted therapies (40). Studies indicate promising effects of histone deacetylase (HDAC) inhibitors (Panobinostat, Fimepinostat) and demethylase inhibitors (GSKJ1 and its prodrug GSKJ4) as monotherapies and in combination with additive beneficial effects (41-44).

In parallel with the nearly global loss of histone trimethylation, studies have found dramatic increases in methylation at hundreds of gene loci, particularly at tumor suppressor genes, which are thereby silenced (28, 29). Polycomb repressor complex 2 (PRC2) has been found to play a key role in the locally increased trimethylation of H3K27 (29). Inhibition of its catalytic subunit, enhancer of zeste 2 (EZH2), as a strategy to restore trimethylation of H3K27 appears to be effective in vitro and in vivo in preclinical studies (42, 45). Paradoxically, one study showed no significant beneficial effect of EZH2 inhibition, raising doubts about its efficacy and indicating that further studies are needed (46).

1.1.10.2 **Growth factors targeted therapies**

Studies indicated frequent up-regulation of growth-factor associated receptor tyrosine kinases (RTKs) involved in RTK-RAS-PI3K-Akt signaling pathway, suggesting that targeted inhibition of RTKs may be useful in the therapy for diffuse midline glioma. In particular PDGFR-alpha, MET, IGF1R, PIK3R1 and PIK3CA are implicated (7, 30-33).

Agents targeting PDGFR, such as imatinib and dasatinib, have shown only modest antitumor activity in clinical trials (47). Other trials have investigated PARP1 inhibitors (olaparib, niraparib, veliparib), CDK4/CDK6 inhibitors (PD-0332991), WEE1 kinase inhibitor (MK1775), and the angiogenesis inhibitor (bevacizumab) all of which failed to show significant efficacy in diffuse midline glioma (8). Overall, the greatest cytotoxic activity was observed with multikinase inhibitors (40).

1.1.10.3 **Immunotherapy**

Chimeric antigen receptor (CAR) T-cell therapy, involving *ex vivo* genetic modification of T cells to target surface antigens on tumor cells, demonstrated potent anti-tumor efficacy in H3K27M+ diffuse midline gliomas. However, it is important to note that, administration of these GD2-CARs resulted in fatal hypercephalus in a subset of animals, so caution should be taken when developing clinical trials (48). In another study, disruption of the CD47 antiphagocytic SIRPα axis by a humanized anti-CD47 antibody yielded promising results against DMG in vivo models. However, the lack of immunocompetent mouse models in this study makes translation into clinical trials rather challenging (49).

To date, current treatment options have either proven insufficient or require additional investigation prior to implementation in clinical trials, underscoring the need for further assessment of novel therapeutic agents.

1.2 Assessment of novel therapeutic agents against DMG

The initial step in any drug screening is determining whether a therapeutic agent displays direct cytotoxic effects or impacts cell proliferation through a cytotoxicity/viability assay (50). There are a variety of methods for measuring cytotoxic and cytostatic effects based on different cell functions such as enzyme activity, cell membrane permeability, cell adherence, adenosine triphosphate (ATP) production, co-enzyme production, and nucleotide uptake activity (50). In this study, we assessed the cytotoxic effects *in vitro* by quantifying ATP - an indicator of metabolically active cells - in the presence or absence of various novel therapeutic candidates against DMG (51).
To predict therapeutic efficacy against DMG, we compared half maximal inhibitory concentrations (IC50) and potency ratios of the therapeutic agents in our panel.

1.2.1 IC50 and potency ratio for predicting therapeutic efficacy

IC50 is defined as the concentration of an agent required to inhibit a given biological activity by half, in our instance, to reduce viability of DMG tumor cells by 50% (52). Hence high therapeutic potential leads to low IC50 values (53). An important limitation in implementing IC50 results from nonclinical experimental designs in clinical trials is the use of concentrations far greater than those that could be realistically achieved in patients (54). To attain therapeutic efficacy in clinical setting the IC50 should be far below the peak concentration (Cmax) — highest concentration reached in the bloodstream after systemic administration (55). Accordingly, we calculated the ICCmax/IC50 ratio (potency ratio) with high therapeutic potential resulting in large potency ratios.

Given the challenges in treating DMG, further drug validation experiments are required to identify drugs that not only effectively target the tumor but also surpass obstacles faced in the clinical setting.

1.2.2 **Treatment challenges and progress barriers**

Diffuse midline glioma has proved challenging to treat. Owing to its eloquent location and infiltrative nature, DMG is inoperable (39).

Previously, diffuse midline glioma was rarely biopsied, limiting the availability of tumor tissue for molecular studies (3, 13, 14). Given the increasing acquirement of post-mortem tissue and biopsies, multiple molecular studies can now be performed, leading to a better understanding of the tumor biology and investigation of novel therapies (8). Nowadays, some of the main treatment challenges facing us in clinical setting are outlined in the following.

1.2.2.1 **Drug-induced neurotoxicity**

Drug safety issues remain one of the leading sources of clinical trial discontinuation (56). In particular, neurotoxic effects caused by chemotherapy or radiation administered during treatment can cause fatal damage with long-term disabling effects, limiting treatment options (57). In this thesis, we addressed the risk assessment of drug induced neurotoxicity of various novel therapeutic candidates. Because conventional animal-based toxicity assays are not only time-consuming and costly, but also require a large number of animals, and the results are only ambiguously transferable to humans, we used pluripotent stem cells (iPSC) to induce human neurons, which we then used for neurotoxicity screening.

1.2.2.2 **Blood brain barrier (BBB) permeability**

Like most primary brain tumors, diffuse midline glioma is protected by the blood-brain barrier (BBB)- a system of tight junctions and transport proteins that acts as a diffusion barrier to shield sensitive neural tissue from potentially harmful substances in the bloodstream (58). A substantial hindrance between clinical application and tumor targets identification is the lack of efficient drug delivery across an intact BBB, limiting the central distribution of drugs that are beneficial to treat DMG (59, 60).

1.2.2.3 **Acquisition of drug and radiation resistance.**

The transient effects of radiotherapy in DMG patients are attributed to radiation resistance mediated by TP53 mutation (61). Furthermore, acquisition of drug resistance via altered mechanisms of cell biology is another complex challenge that is best addressed with combination therapy and requires further, more in-depth experiments (62).

1.2.2.4 **Diffuse midline glioma microenvironment**

Another aspect that should be given greater consideration when deciding on treatment for DMG is the microenvironment. Studies have concluded that DMG has neither a highly immunosuppressive nor inflammatory microenvironment, thus displaying a distinct tumor microenvironment that differs strikingly from that of adult GMB (63, 64).

2. *Material and Methods*

2.1 **Cytotoxicity-Assay**

2.1.1 ***In vitro* cultivation of DMG-cell lines**

We tested on five patient-derived DIPG suspension cell lines. Of these, four cell lines (DIPGXIII, DIPG007, DIPGXIIIP *, BT869) harbor a K27M mutation in H3.3 and one cell line (DIPG SUIV) in H3.1. All DIPG cell lines were grown in a tumour stem cell media consisting of a 1:1 solution of Dulbecco's Modified Eagles Medium: Nutrient Mixture F12 (DMEM/F12) and Neurobasal-A Medium, supplemented with 1 M HEPES solution, 100 nM sodium pyruvate solution, 10 mM non-essential amino acids solution, 1x Glutamax-I Supplement and 1x Antibiotic- Antimycotic solution. Tumour stem cell medium solution was additionally supplemented with 1X B-27 Supplement minus Vitamin A and 20 $ng \cdot mL^{-1}$ Human-EGF (AF-100-15), 20 $ng \cdot mL^{-1}$ Human-FGF-basic, 20 $ng \cdot mL^{-1}$ Human-PDGF-AA, 20 $ng \cdot mL^{-1}$ Human-PDGF-BB and 2 $\mu g \cdot mL^{-1}$ Heparin solution. (65) Cells were cultured at 37°C in a humidified 5% atmosphere.

2.1.2 **Seeding DMG-cells**

Tumor cells were transferred to a 50 ml Falcon tube and centrifuged at 300 g for 5 min at room temperature. The cell sediment was than dissociated into single cells using 1 ml of enzymatically active TrypLE for 3 min at room temperature. After resuspending the sediment in DMEM / F12, large debris and non-separated cell clumps were removed with a 70 µm cell strainer. The remaining suspension was centrifuged for 5 min at room temperature at 300 g to pellet the separated cells. The cell sediment was resuspended in the tumour stem cell medium and the cells were counted with the help of tryptan blue 0.4% solution. The cells were seeded in 384 well plates using the ASSIST pipetting robot in the following densities: DIPGXIII – 1000cpw; BT869– 1000 cpw; DIPG007 – 1000cpw, DIPGXIIIP* - 1000 cpw and DIPG-SUIV 1000 cpw. Cells were than incubated overnight at 37 °C in 5% CO2.

2.1.3 **DMG-cell treatment**

Twenty-four hours after cell seeding, DMG cells were exposed to the selected chemotherapeutic agents. Initially, the investigated agents were manually diluted in DMEM/F12 in a 96-well V-bottom plate at the highest concentration required for the assay. Each of these master plates included a negative control (treatment with 99.9% DMSO), to which the treated cells were compared. A ten-fold serial dilution was then performed using the ASSIST pipetting robot, resulting in six different concentrations of each chemotherapeutic agent. Using the ASSIST pipetting robot, each quadrant of each 384-well plate containing DMG cells was treated with one master plate, resulting in simultaneous treatment of every cell line with 28 agents at six concentrations per experiment. Treated cells were incubated for 72 hours at 37°C in a humidified 5% atmosphere.
Thirty agents were screened using this approach, including five HSP90 inhibitors, five microtubule targeting agents, three proteasome inhibitors, two alkylating agents, two CDK-Inhibitors, two dual inhibitors of PI3K and mTOR, two NAMPT inhibitors, two DRD2 antagonist and ClpP agonist and seven HDAC inhibitors, one of which, CUCD 907, also acts as a PI3K inhibitor.

2.1.4 **Cell Titer-Glo luminescent cell viability assay**

At 72 hours after treatment, the viability of DMG cells and thus the cytotoxicity of the tested agents was assessed using the Cell Titer-Glo luminescence cell viability assay. 20µl of the Cell Titer-Glo reagent was added to each well, and luminescence was measured using the microplate reader Varioskan LUX Multimode and the SkanIt Microplate Reader Software. Tumor cell viability was expressed relative to DMSO control.

2.1.5 **Curve fitting of the IC50 data**

Curve fitting to determine IC50 values was performed with GraphPad Prism via a nonlinear regression of "log(inhibitor) vs. response - variable slope (four parameters)".

2.2 Human Induced Pluripotent Stem Cells (iPSC) Culture

Human Induced Pluripotent Stem Cell (iPSC) handling was performed under sterile conditions according to the manufacturer's instructions with minor modifications (66).

2.2.1 Human iPSCs Maintenance

Human Induced Pluripotent Stem Cells (iPSCs) were cultured under sterile conditions on Matrigel-coated 6-well culture vessels in stabilized, feeder-free mTeSR Plus medium. mTeSR Plus medium consists of a 1:4 solution of mTeSR Plus supplement and mTeSRTM Plus basal medium, both thawed overnight at 4 °C prior to mixing. Medium changes were performed every other day according to the manufacturer's instruction. Cells were cultured at 37 °C in a humidified atmosphere containing 5% CO2.

2.2.2 Coat culture vessels with Matrigel

To mimic the *in vivo* environment for our cell culture, we coated our culture vessels with Matrigel.

Vials containing Corning Matrigel hESC-qualified, LDEV-free matrix were thawed overnight at 2-8 °C, sterile aliquoted, and stored at -20 °C. Prior to coating, Matrigel aliquots were thawed and diluted 1:100 with cold advanced DMEM/F12 on ice. The surface of each culture vessel was quickly covered with the diluted Matrigel solution and subsequently incubated at 37 °C and 5% CO2 for at least 1 hour. The required volume of the matrigel solution was adjusted for each culture vessel according to the manufacturer's recommendations. For overnight storage, the culture vessels were sealed with Parafilm laboratory film to prevent drying. Prior to use, the Matrigel solution was aspirated from the culture vessels whereupon the cells were plated directly onto the coated culture vessels without rinsing.

2.2.3 **Freezing human iPSCs**

Human iPSCs were frozen only once they reached 60 – 80 % confluency. Spent media was aspirated from each well containing iPSCs. Wells were afterwards rinsed with pre-warmed PBS to eliminate any dead cells or debris. Next, 1mL of enzyme-free ReLeSR reagent was added to dissolve the iPSC colonies into clumps of cells without the need for manual selection or scraping. Following an incubation period of 5 - 7 minutes at 37°C, 2 mL of DMEM/F12 with HEPES were added to each well, whereupon the iPSCs were cautiously washed using a 5 ml serological pipette. By gently tapping the side of the plate for approximately 30-60 seconds, colonies were further detached and then transferred to a 15-mL conical tube. Cells were centrifuged at 300xg for 5 min, after which the supernatant was aspirated and discharged. The cell pellet was then resuspended very gently in cold Bambanker Freezing Solution. One ml of cell suspension was dispensed to each cryotube and cells were frozen overnight at -80 °C in corning cool cell containers. Afterwards the tubes were transferred into a - 80 °C freezer for long-term storage.

2.2.4 **Thawing cryopreserved iPSCs**

Initially, 1.5 mL of mTeSR plus supplemented with 10 µM of ROCK inhibitor Y27632 was added to a Matrigel-coated 6-well culture vessel, which was subsequently incubated at 37 °C in a humidified atmosphere containing 5% CO2. Cryovials containing frozen iPSCs were thawed in a 37 °C water bath for approximately 1-2 minutes and transferred to pre-warmed Advanced DMEM/F12 medium. The resulting suspension was centrifuged at 300xg for 5 minutes. The supernatant was aspirated and discarded whereas the pellet was resuspended in mTeSR Plus. Lastly, 500µl of the cell suspension was added to each well, resulting in a final volume of 2 mL per well. After twenty-four hours, a complete medium change was performed to remove the ROCK inhibitor Y27632. For more information on the further handling of iPSCs, refer to “Human iPSCs Maintenance”.

2.3 Human iPSC- derived neural cultures

2.3.1 Induction of Neural Stem Cells from Human Pluripotent Stem Cells

The induction of Neural Stem Cells (NSCs) from human iPSCs was performed according to the manufacturer's instructions with minor modifications (67). All steps were performed under sterile conditions.

2.3.1.1 IPSC subculturing

When the confluency of iPSCs reached approximately 70-80%, medium was removed from each well and 1mL of ReLeSR was added to dislodge the iPSC colonies into clumps of cells. After an incubation period of 5 - 7 minutes at 37°C, 1 mL of mTeSR was added to each well. By gently tapping the side of the plate for approximately 30-60 seconds, colonies were detached and subsequently transferred to a 15-mL conical tube. The cell aggregate mixture was plated at about 15 – 25% confluency onto a coated 6-well plate containing 1 mL mTeSR plus supplemented with 10 µM of ROCK inhibitor Y27632. The plate was moved in several rapid, short back-and-forth and sideways movements to uniformly distribute the cell aggregates. The cell culture plate was incubated at 37°C in a humidified 5% atmosphere for twenty-four hours before being inducted in NSCs.

2.3.1.2 NSC derivation from PSC

On day one of iPSC splitting, the spent medium was aspirated to remove non-adherent cells and eliminate the ROCK inhibitor. 2.5 ml of pre-warmed PSC Neural Induction medium consisting of Neurobasal Medium mixed with 2x Neural Induction Supplement was added to each well. 48 hours later, we repeted the complete medium change as on day one of iPSC splitting. On the fourth and sixth days of neural induction, the spent medium was aspirated from each well and 5 ml of pre-warmed PSC Neural Induction Medium was added per well as the cell density in the culture was very high with cells reaching confluency from day 4 onwards.

2.3.1.3 **NSC harvesting and expansion prior to cryopreservation**

On day 7 of neural induction, the NPCs (P0) were passaged prior to expansion (P1). The spent PSC neural induction medium was aspirated from the 6-well plate to be passaged, and the cells were carefully rinsed with Dulbecco's phosphate-buffered saline (DPBS) without $CaCl_2$and $MgCl_2$. To detach the cells from the surface of the culture vessel, 1 ml of pre-warmed StemPro Accutase Cell Dissociation Reagent was added to each well of the 6-well plates and incubated at 37°C for 5 - 8 minutes. The resulting cell suspension was transferred to a 15-mL conical tube and mixed gently with a pipette to break up cell clumps. The cell suspension was filtered through a 100-µm strainer and centrifuged at 300 × g for 4 minutes. After aspirating and discharging the supernatant, the cell pellet was rinsed in DPBS and centrifuged again at 300 × g for 4 min to remove remaining dead cells and debris. The cell pellet was resuspended in prewarmed neural expansion medium consisting of a 1:1 solution of Neurobasal medium and Advanced DMEM/F-12 supplemented with 2x Neural Induction Supplement. After determining the cell concentration and supplementing the suspension with 10 µM of ROCK inhibitor Y27632, 5 × 10^5 cells / well were plated in a 6-well Matrigel-coated plate. The plate was moved in several rapid, short back-and-forth and side-to-side movements to evenly distribute the cells. The cell culture plate was incubated at 37°C in a humidified 5% atmosphere for twenty-four hours by which time the spent medium was removed and replaced with fresh neural expansion medium to eliminate the ROCK inhibitor Y27632. A complete medium change was performed every other day onward.

2.2.2.5. **Cryopreservation of NSCs**

When the NSCs reached confluency, the spent medium was aspirated from each well and 1 ml of pre-warmed Accutase Reagent was added to and incubated at 37 °C for 3 - 5 minutes to dislodge the cells from the surface of the culture vessel. The cell suspension was transferred to a 15-mL conical tube. The wells were gently rinsed with DPBS, and the remaining cells were collected and likewise transferred to the same 15-ml conical tube. The resulting cell suspension was mixed carefully with a pipette to break up cell clumps and centrifuged at 300 × g for 4 minutes. After aspirating and discharging the supernatant, the cell pellet was

rinsed in DPBS and centrifuged again at 300 × g for 4 min to remove remaining dead cells and debris. The cell pellet was resuspended in pre-warmed neural expansion medium, and the cell concentration was determined. Lastly, the suspension was diluted in neural progenitor cell freezing medium at a cell concentration of 2.5×10^6 cells / mL. One ml of cell suspension was dispensed to each cryotube and cells were frozen overnight at -80 °C in corning cool cell containers. Afterwards the tubes were transferred into a - 80 °C freezer for long-term storage.

2.3.2 **Differentiation of neuronal network cultures from iPSC- derived NSCs**

Differentiation of neural network cultures from human iPSC - derived NSCs was performed under sterile conditions according to the manufacturer's instructions with minor adjustments (68).

2.3.2.1 **Coating culture vessels with poly-L-ornithine**

The poly-L-ornithine (PLO) solution was diluted in PBS to a concentration of 15 µg/ml, of which 150 µl/cm^2 was used to coat the surface of Nunc-treated cell culture plates. Culture vessels were incubated with the thin layer of PLO for two hours at 37°C in a humidified 5% atmosphere. Subsequently, the PLO solution was removed, and the culture vessels were thoroughly rinsed three times with PBS to eliminate toxic poly-L-ornithine residuals.

2.3.2.2 **Coating culture vessels with laminin**

Laminine was thawed at 4 ° C and diluted 1:200 with DMEM/F12. 150 µl/cm^2 of the laminin solution was added into PLO-coated plates and incubated at 37°C in a humidified 5% atmosphere for two hours. Just prior to use, the laminin solution was aspirated from each well. Cells were plated directly onto the laminin-coated plates without rinsing.

2.3.2.3 **Recovering and plating cryopreserved NPCs**

Cryopreserved NSCs were thawed in a 37 ° C water bath and added to pre-warmed DMEM/F12. The resulting suspension was centrifuged at 300g for 5 minutes. The supernatant was discharged, and cells were resuspended in Neural Expansion Medium supplemented with 10 µM of ROCK inhibitor Y27632. Cells

were counted using 0.4% trypan blue solution and the cell concentration was adjusted so that 5 x 10^4 cells / cm^2 were plated on the PLO/laminin-coated plates. Cells were then incubated overnight at 37°C in a humidified 5% atmosphere.

2.3.2.4 **Early neuron differentiation**

On day 1 of NSC plating, the spent medium was removed and replaced with ~ 250 µl/cm^2 fresh neural differentiation medium, consisting of a 1:1 solution of Neurobasal-A Medium and DMEM/F12 with GlutaMAX, supplemented with 2 ng·mL^{-1} laminin, 20 ng·mL^{-1} brain-derived neurotrophic factor (BDNF), 10 ng·mL^{-1} glial cell derived neurotrophic factor (GDNF); 1 µM dibutyryl cAMP, 200 µM ascorbic acid, 1x N2-supplement, 1 x B27 supplement without vitamin A and 1 x 5.000 U/mL Penicillin-Streptomycin solution. The medium was additionally supplemented with 1 x Culture One Supplement to prevent overgrowth of contaminating progenitor cells while simultaneously efficiently maintaining the population of neurons (69). On day 3 of NSC plating, 250 µl/cm^2 fresh neural differentiation medium was added without removing the spent media. Every second day a half medium change was performed.
Daily phase contrast imaging and neurite length analysis were obtained using a live-cell imaging and analysis platform, the IncuCyte, to monitor early neuron differentiation and determine the optimal timing for further testing.

2.4 **Neurotoxicity assay**

To predict the neurotoxic treatment-related side effects of the selected drugs in our panel, we conducted a label-free neurotoxicity assay. In this experiment, the dynamic changes in neurite length of iPSC-derived neural network cultures cultivated in 48 well plates were compared with a negative control over a period of 7 days after treatment. Prior to treatment, the spent medium was removed from all wells and 150 µl of fresh neural differentiation medium was added to each well. Next, the plates were imaged to assess the pre-treatment neurite length. Pre-treatment measurements also ensured that control and test wells were equivalent prior to drug exposure. Immediately afterwards the wells were treated with the IC50 and cmax concentration of each drug. Wells treated with 10 nM DMSO served as negative control. The plate was imaged every 3 hours with the phase-

contrast channel in the IncuCyte Live-Cell Analysis System with a 20× objective (9 images per well) using neuro-track analyses “Neurite Backgr. 0,6; 1µm N width; 0,25 sensitivity” to measure neurite length per image area expressed as mm/mm^2 image area.

2.5 **Immunofluorescence staining**

iPSC-derived neural stem cells (NSCs) were plated in an 8-well Matrigel-coated chamber slide immediately after recovery from cryopreservation at a density of 10^5 cells / cm^2 and 2×10^5 cells / cm^2. Staining of pluripotent markers (Nestin, Sox-2, and Pax-6) was performed on day 1 of NSC plating. In contrast, iPSC-derived early neurons were differentiated from NPCs for 7 days in an 8-well PLO/LC-coated chamber slide, at a density of 5 x 10^5cells / cm^2 and 7 x 10^5 cells / cm^2 according to the protocol “Differentiation of neuronal network cultures from iPSC- derived NSCs” and subsequently stained for early neuron markers (Tuj1, MAP2) and for the astrocyte cell marker GFAP.

Initially, both iPSC-derived neuronal cultures were carefully washed twice with PBS, with each rinse lasting 10 minutes, to remove any residual debris. Subsequently, the cells were fixated with 4% paraformaldehyde (PFA) in 0.1 M phosphate buffer for 15 minutes at RT, whereupon the coverslips were rinsed 3 times with PBS, with 5 minutes per rinse, at RT. Afterwards, cells were incubated with 0.5 mL permeabilization and blocking buffer (0.3% Triton X-100, 5% BSA and 2 % FBS in PBS), which was placed to each well for one hour at RT. Next, the coverslips were incubated overnight in a humid chamber at 4 ° C with 125 µL of a suspension solution of the primary antibody diluted in an antibody dilution solution (ADS) consisting of 0,3 % Triton X-100 with 1 % BSA in PBS. The primary antibodies were added as follows: mouse anti - βIII tubulin (TUJ1) at a final dilution of 1:100, mouse anti - GFAP at a final dilution of 1:100, mouse anti – SOX 2 at a fnal dilution of 1:50, rabbit anti – PAX 6 at a final dilution of 1:100, rabbit anti – MAP 2 at a final dilution of 1:100, rabbit anti – Nestin at a final concentration of 1:2000.

Subsequently, coverslips were rinsed 2 times with PBS with 5 minutes per rinse at room temperature. Next, coverslips were incubated with 125 µL of Alexa Fluor

488- or 594-conjugated goat anti-mouse or anti-rabbit IgG secondary antibody, at a final concentration of 1:200 for 2 hours at RT in a dark, humid chamber. The washing procedure was repeated three times with DPBS, with 5 minutes per rinse. Nuclear mounting was carried out by incubating the coverslips with 4,6-diamid-ino-2-phenylindole (DAPI) at a concentration of 10 nM at RT in the dark. The coverslips were air dried overnight in the dark and sealed with nail polish before imaging. For long term storage, the cover slides were kept at 4 ° C in the dark.

2.6 Statistical analysis

All data are shown as the mean ± standard deviation (SD) of three independent experiments and performed with GraphPad Prism.

2.7 List of compounds and materials used throughout the thesis

Table 1: *List of the chemotherapeutic agents screened and their mechanism of act. The supplier and catalog/part number are also given.*

Chemotherapeutic agent	Mechanism of action	Supplier and catalog number
AUY922	HSP90 inhibitor (70)	Adooq Bioscience; A10659
Azixa (MPC6827)	Mitosehemmer (71)	RayBiotech; 331-22085
Belinostat	HDAC inhibitor (72)	MCE*; HY-10225
Carfizomib	Irreversible proteasome inhibitor (73)	MCE*; HY-10455
Combrestastatin A4	Inhibits tubulin polymerization → disruption in microtubule dynamics (74)	Selleckchem; S7783
CUDC907	PI3K-Inhibitor & HDAC-inhibitor (75)	MCE*; HY-13522
Daporinad	NAMPT inhibitor (76)	MCE*; HY-50876
Delanzomib	Proteasome inhibitor (77)	TargetMol; T6027
Dinaciclib	Multi CDK-Inhibitor: selective CDK1, CDK2, CDK5, and CDK9 inhibitor (78)	Adooq Bioscience; A11129
Entinostat	HDAC inhibitor (72)	MCE*; HY-12163
GDC0084	PI3K inhibitor & mTOR inhibitor (79)	MCE*; HY-19962
Gedatolisib	PI3K inhibitor & mTOR inhibitor (80)	TargetMol; T1970
Geldanamycin	HSP90 inhibitor (70)	TargetMol; T6342
GMX-1778	NAMPT inhibitor (81)	TargetMol; T1998
HSP-990	HSP90 inhibitor (70)	Adooq Bioscience; A12850
4- Hydroxy-lomustin	Alkylating agent (82)	Toronto Research Chemicals; H942990
Marizomib	Pan-proteasome inhibitor (83)	Adooq Bioscience; A13853

MTIC	Alkylating agent (84)	TorontoResearchChemicals; M760000
Ombrabulin	Inhibits tubulin polymerization → destabilizes the microtubules (85)	MCE*; HY-18256
Onalespib	HSP90 inhibitor (70)	MCE*; HY-14463
ONC 206	Activator of ClpP and selective antagonist of the DRD2/3/4 (86)	MCE*, HY135147
Panobinostat	HDAC inhibitor (72)	MCE*; HY-10224
Quisinostat	HDAC inhibitor (72)	MCE*; HY-15433
Romidepsin	HDAC inhibitor (72)	MCE*; HY-15149
SNX-2112	HSP90 inhibitor (87)	Adooq Bioscience; A11189
Staurosporine	Multi phosphokinase inhibitor ** (88)	MCE*; HY-15141
TIC-10	Activator of ClpP and selective antagonist of the DRD2/3/4 (86)	TargetMol; T7001
Vincristine	inhibits microtubule formation → prevents formation of the mitotic spindle (89)	MCE*; HY-N0488
Vinorelbine	inhibits microtubule formation → prevents formation of the mitotic spindle (90)	MCE*; HY-12053
Vorinostat	HDAC-1, -2, and- 3 (Klasse I) – as well as HDAC-6 (Klasse II) inhibitor (72)	MCE*; HY-10221

* MCE – Medchemexpress

** Nonspecific inhibitor of many phosphokinases (serine/threonine kinase AKT, calcium-dependent protein kinase C, and cyclin-dependent kinases) (88).

Table 2: *List of compounds and materials used throughout the thesis. The supplier and catalog/part number are also given.*

Compound / material	Supplier and catalog / part number
Neurobasal-A Medium	Thermo Fisher Scientific, cat. no. 10888-022
DMEM/F-12	Thermo Fisher Scientific, cat. no. 11330-032
HEPES Buffer Solution (1M)	Thermo Fisher Scientific, cat. no. 15630-080
Sodium Pyruvate (100 mM) (100X)	Thermo Fisher Scientific, cat. no. 11360-070
MEM Non-Essential Amino Acids Solution (MEM NEAA) (100X)	Thermo Fisher Scientific, cat. no. 11140-035
GlutaMAX-I Supplement (100x)	Thermo Fisher Scientific, cat. no. 35050-061
Antibiotic-Antimycotic (100X)	Thermo Fisher Scientific, cat. no. 15240-062
B-27 Supplement without Vitamin A (50x)	Thermo Fisher Scientific, cat. no. 12587001
hEGF	BIOZOL, cat. no. SHD-100-26
hFGF-basic-154	PeproTech, cat. no. 100-18B
hPDGF-AA	PeproTech, cat. no. 100-13A
HPDGF-BB	PeproTech, cat. no. 100-14B
Heparin Solution (0.2%)	STEMCELL Technologies, cat. no. 7980
Dimethylsulfoxid (DMSO), sterile	Sigma Aldrich, cat. no.: D2650
TrypLE™ Express Enzyme (1X), no phenol red	GIBCO, cat. no.: 12604013
70 µm cell strainer	VWR, cat. no.: 732-2758
100 µm cell strainer	VWR, cat. no.: 732-2759

Trypan Blue Solution, 0.4%	Thermo Fisher Scientific, cat. no. 15250061
Advanced DMEM/F-12	Thermo Fisher Scientific, cat. no. 12634010
Costar 48-well Clear TC-treated Multiple Well Plates, Individually Wrapped, Sterile	Corning, cat. no.: 3548
Costar 6-well Clear TC-treated Multiple Well Plates, Individually Wrapped, Sterile	Corning, cat. no.: 3516
Corning Osteo Assay Surface 96-well Multiple Well Plates, Individually Wrapped, Sterile	Corning, cat. no.: 3988
Cryotubes, self-standing, 2 ml	VWR, cat. no.: 479-1262
Single Channel EVOLVE Pipettes, volume range 0.2 – 2 µl	Integra-Biosciences, part no.: 3011
Single Channel EVOLVE Pipettes, volume range 1 – 10 µl	Integra-Biosciences, part no.: 3012
Single Channel EVOLVE Pipettes, volume range 2 – 20 µl	Integra-Biosciences, part no.: 3013
Single Channel EVOLVE Pipettes, volume range 10 – 100 µl	Integra-Biosciences, part no.: 3015
Single Channel EVOLVE Pipettes, volume range 20 – 200 µl	Integra-Biosciences, part no.: 3016
Single Channel EVOLVE Pipettes, volume range 100 – 1000 µl	Integra-Biosciences, part no.: 3018
Single Channel VIAFLO Pipettes; volume range 0.5 – 12.5 µl	Integra-Biosciences, part no.: 4011
Single Channel VIAFLO Pipettes; volume range 5 – 125 µl	Integra-Biosciences, part no.: 4012
Single Channel VIAFLO Pipettes; volume range 10-300 µl	Integra-Biosciences, part no.: 4013
Single Channel VIAFLO Pipettes; volume range 50-1250 µl	Integra-Biosciences, part no.: 4014
Griptip size 12.5 µl, sterile, racks of 384Tips	Integra-Biosciences, part no.: 4414
Griptip size 125 µl, sterile, racks of 384 Tips	Integra-Biosciences, part no.: 4424
Griptip size 300 µl, sterile, racks of 96 Tips	Integra-Biosciences, part no.: 4434
Griptip size 1250 µl, sterile, racks of 96 Tips	Integra-Biosciences, part no.: 4444
ASSIST PLUS pipetting robot, incl. tip waste bin, pipette charging cable	Integra-Biosciences, part no.: 4505
8-Channel VOYAGER adjustable tip spacing pipette, volume range 0.5 – 12.5 µl	Integra-Biosciences, part no.: 4721
8-Channel VOYAGER adjustable tip spacing pipette, volume range 5-125 µl	Integra-Biosciences, part no.: 4722
8-Channel VOYAGER adjustable tip spacing pipette, volume range 10-300 µl	Integra-Biosciences, part no.: 4723
8-Channel VOYAGER adjustable tip spacing pipette, volume range 50-1250 µl	Integra-Biosciences, part no.: 4724
Griptip for VOYAGER pipette, size 12.5 µl long, sterile, racks of 384 Tips	Integra-Biosciences, part no.: 6404
Griptip for VOYAGER pipette, size 125 µl, sterile, racks of 384 Tips	Integra-Biosciences, part no.: 6464
Griptip for VOYAGER pipette, size 300 µl, sterile, racks of 96 Tips	Integra-Biosciences, part no.: 6434
Griptip for VOYAGER pipette, size 1250 µl, sterile, racks of 96 Tips	Integra-Biosciences, part no.: 6444
10 ml, Disposable Reservoirs, 1 Sleeve of 50, Sterile, Polystyrene, SureFlo™ anti-sealing array	Integra-Biosciences, part no.: 4373
100 ml, Disposable Reservoirs, 1 Sleeve of 50, Sterile, Polystyrene, SureFlo™ anti-sealing array	Integra-Biosciences, part no.: 4393
Screw cap tube, 15 ml, (LxØ): 120 x 17 mm, PP, with print	Sarstedt, order-no.: 62.554.502

Screw cap tube, 50 ml, (LxØ): 114 x 28 mm, PP, with print	Sarstedt, order-no.: 62.548.004
Filtropur V25, Vacuum filtration unit, 250 ml, PES, 0.2 µm	Sarstedt, order-no.: 83.3940.001
Filtropur V50, Vacuum filtration unit, 500 ml, PES, 0.2 µm	Sarstedt, order-no.: 83.3941.001
Filtropur V100, Vacuum filtration unit, 1000 ml, PES, 0.22 µm	Sarstedt, order-no.: 83.3942.001
Serological pipette, plugged, 50 ml, sterile, non-pyrogenic/endotoxin-free, non-cytotoxic, 1 piece(s)/blister	Sarstedt, order-no.: 86.1256.001
Serological pipette, plugged, 25 ml, sterile, non-pyrogenic/endotoxin-free, non-cytotoxic, 1 piece(s)/blister	Sarstedt, order-no.: 86.1685.001
Serological pipette, plugged, 10 ml, sterile, non-pyrogenic/endotoxin-free, non-cytotoxic, 1 piece(s)/blister	Sarstedt, order-no.: 86.1254.001
Serological pipette, plugged, 5 ml, sterile, non-pyrogenic/endotoxin-free, non-cytotoxic, 1 piece(s)/blister	Sarstedt, order-no: 86.1253.001
PIPETBOY acu 2 mains adapter, spare sterile filter 0.45 µm and wall mount, blue	Integra-Biosciences, part no.: 155 017
PIPETBOY acu 2 mains adapter, spare sterile filter 0.45 µm and wall mount, red	Integra-Biosciences, part no.: 155 016
Aspiration pipette, unpadded, 2 ml, sterile, non-pyrogenic/endotoxin-free	Sarstedt, order-no: 861.252.011
Neurobasal Medium	Thermo Fisher Scientific, cat. no. 21103-049
Advanced DMEM/F12	Thermo Fisher Scientific, cat. no. 12634-010
Neural Induction Supplement (50X)	Thermo Fisher Scientific, cat. no. A1647701
DMEM/F12+GlutaMAX	Thermo Fisher Scientific, cat. no. 31331028
Neurobasal-A Medium	Thermo Fisher Scientific, cat. no. 10888022
N-2 Supplement (100X)	Thermo Fisher Scientific, cat. no. 17502001
B-27 Supplement without Vitamin A (50x)	Thermo Fisher Scientific, cat. no. 12587001
Laminin	Corning; cat. no. 354232
Recombinant Human/Murine/Rat BDNF	Peprotech, cat. no.: 450-02
Recombinant Human GDNF	Peprotech, cat. no.: 450-10
DcAMP	Sigma Aldrich, cat. no.: D0627
Ascorbic Acid	Sigma Aldrich, cat. no.: A8960
CultureOne Supplement (100X)	Thermo Fisher Scientific cat. no. A3320201
Penicillin-Streptomycin (5.000 U/mL)	Thermo Fisher Scientific cat. no. 15070-063
Corning Matrigel Matrix hESC-Qualified Matrix, LDEV-free	Corning Life Sciences, cat. no.: 354277
Parafilm	Sigma Aldrich, cat. no. P7793-1EA
ReLeSR (Passaging Reagent)	Stem Cell Technologies cat. no.: 05872
mTeSR Plus	Stem Cell Technologies cat. no.: 05825
ROCK inhibitor Y27632	Sigma-Aldrich, cat. no.: Y0503
PSC Neural Induction Medium (consists of Neurobasal® Medium and Neural Induction Supplement, 50X)	Thermo Fisher Scientific cat. no. A1647801
Advanced DMEM⁄F-12	Thermo Fisher Scientific cat. no. 12634
DPBS without $CaCl_2$and $MgCl_2$	Thermo Fisher Scientific cat. no. 14190
Phosphate buffered saline (PBS), pH 7.4	Thermo Fisher Scientific cat. no. 10010002
Phosphate buffered saline (PBS), pH 7.2	Thermo Fisher Scientific cat. no. 70013-016
StemPro Accutase Cell Dissociation Reagent	Thermo Fisher Scientific cat. no. A11105

Corning Cool Cell Containers	Corning, cat. no. 432000
Neural Progenitor Freezing Medium	Stem Cell Technologies cat. no.: 05838
Chamber slide with a removable 8 well silicone chamber	Ibidi, cat. no.: 80841
Anti-GFAP antibody, mouse monoclonal	Abcam, cat. no. Ab10062
Purified anti-Tubulin β 3 (TUJ1) antibody, mouse	Biolegend, cat. no.: 801201
Purified anti-Pax-6 Antibody, Rabbit Polyclonal IgG	Biolegend, cat. no.: 901301
MAP2 Polyclonal Antibody, host: rabbit	Invitrogen, cat. no.: PA5-17646
Nestin Polyclonal Antibodyr, host: rabbit	Invitrogen, cat. no.: PA5-82905
Sox-2 Antibody, host: mouse	Santa Cruz, cat. no.: sc-365964
Goat anti-Rabbit IgG (H+L), Superclonal™ Recombinant Secondary Antibody, Alexa Fluor 555	Invitrogen, cat. no.: A27039
Goat anti-Rabbit IgG (H+L) Highly Cross-Adsorbed Secondary Antibody, Alexa Fluor Plus 488	Invitrogen, cat. no.: A32731
Goat anti-Mouse IgG (H+L) Cross-Adsorbed Secondary Antibody, Alexa Fluor 555	Invitrogen, cat. no.: A21422
Goat anti-Mouse IgG (H+L) Cross-Adsorbed Secondary Antibody, Alexa Fluor 488	Invitrogen, cat. no.: A11001
Paraformaldehydlösung, 4 % in PBS	Thermo Fisher Scientific, cat. no.: 15670799
Triton X-100 Surfact-Amps Detergent Solution	Thermo Fisher Scientific, cat. no.: 11358311
Bovine Serum Albumin (BSA)	Tocris, cat. no.: 5217
Fetal bovine serum (FBS)	Sigma-Aldrich, cat. no.: 06693
Fluoroshield mit DAPI	Sigma-Aldrich, cat. no.: F6057
Poly-L-Ornithine Solution (0.01%)	Sigma-Aldrich, cat. no.: A004C
Laminin Mouse Protein, Natural	Thermo Fisher Scientific, cat. no.: 23017015
Ethanol, 5 l, ≥99,8 %, denatured	Carl Roth, cat. no.: K928.4
Bambanker, Cryopreservation media	Nippon Genetics Europ, cat. no. BB01
Varioskan LUX Multimode Microplate reader	Thermo Fisher Scientific, part no.: VL0L00D0
TSX Series Ultra-Low Freezer	Thermo Fisher Scientific, cat. no.: TSX50086A
BZ-X Series All-in-one Fluorescence Microscope X800	Keyence, part.no.: BZ-X800
Countess 3 FL Automated Cell Counter	Thermo Fisher Scientific, cat. no.: A50299

3. Results

3.1 Assessment of the half-maximal inhibitory drug concentration for DMG-cell lines

Thirty chemotherapeutic agents were screened for their anti-tumor cytotoxic effects, including five HSP90 inhibitors, five microtubule targeting agents, three proteasome inhibitors, two alkylating agents, two CDK-Inhibitors, two dual inhibitors of PI3K and mTOR, two NAMPT inhibitors, two dual DRD2 antagonist and ClpP agonist and seven HDAC inhibitors, one of which, CUCD 907, also acts as a PI3K inhibitor. DMG suspension cells were treated with at least 6 doses of each chemotherapeutic agent and analyzed for viability 72 hours after treatment. The values of each drug concentration were normalized to the control (0.1% DMSO) and expressed as a percentage.

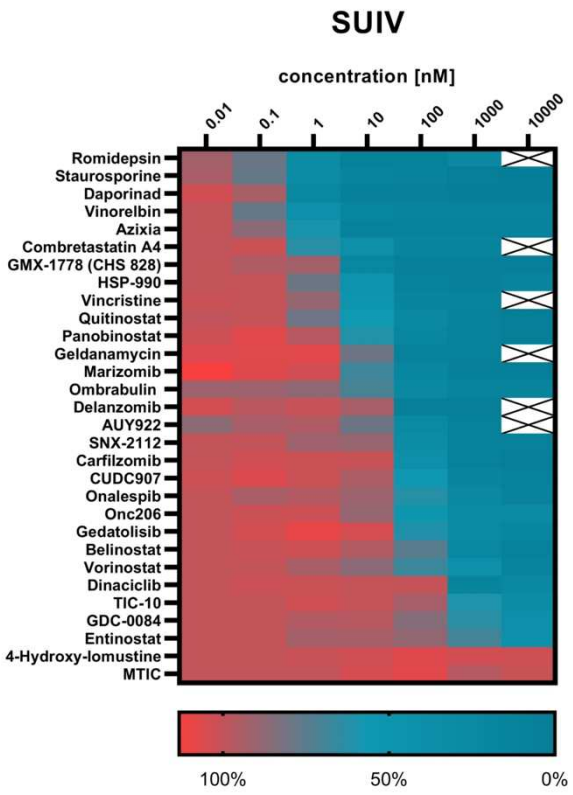

Figure 1: *In the above clustered heatmap, each column represents a concentration in nanomolar, and each row indicates the viability of DMG tumor cells 72 hours after treatment with the chemotherapeutic agents in the left, normalized to the control (0,1%DMSO) and expressed as a percentage. The SUIV-DMG-cell line is H3K27M-mutant with alteration in the histone variant H3.1.*

Anti-tumor cytotoxic activity was estimated based on the half-maximal inhibitory drug concentration (IC50), which is defined as the concentration of an agent required to inhibit a given biological activity by half, in our instance, to reduce the viability of DMG tumor cells by 50% (52). This means that a high therapeutic potential leads to low IC50 values and vice versa (53).

The anti-tumor cytotoxic effects of the agents in our panel were investigated on five patient derived DMG-cell lines, four of which harbor an H3K27M-muatation in the histone variant H3.3 and one in H3.1.

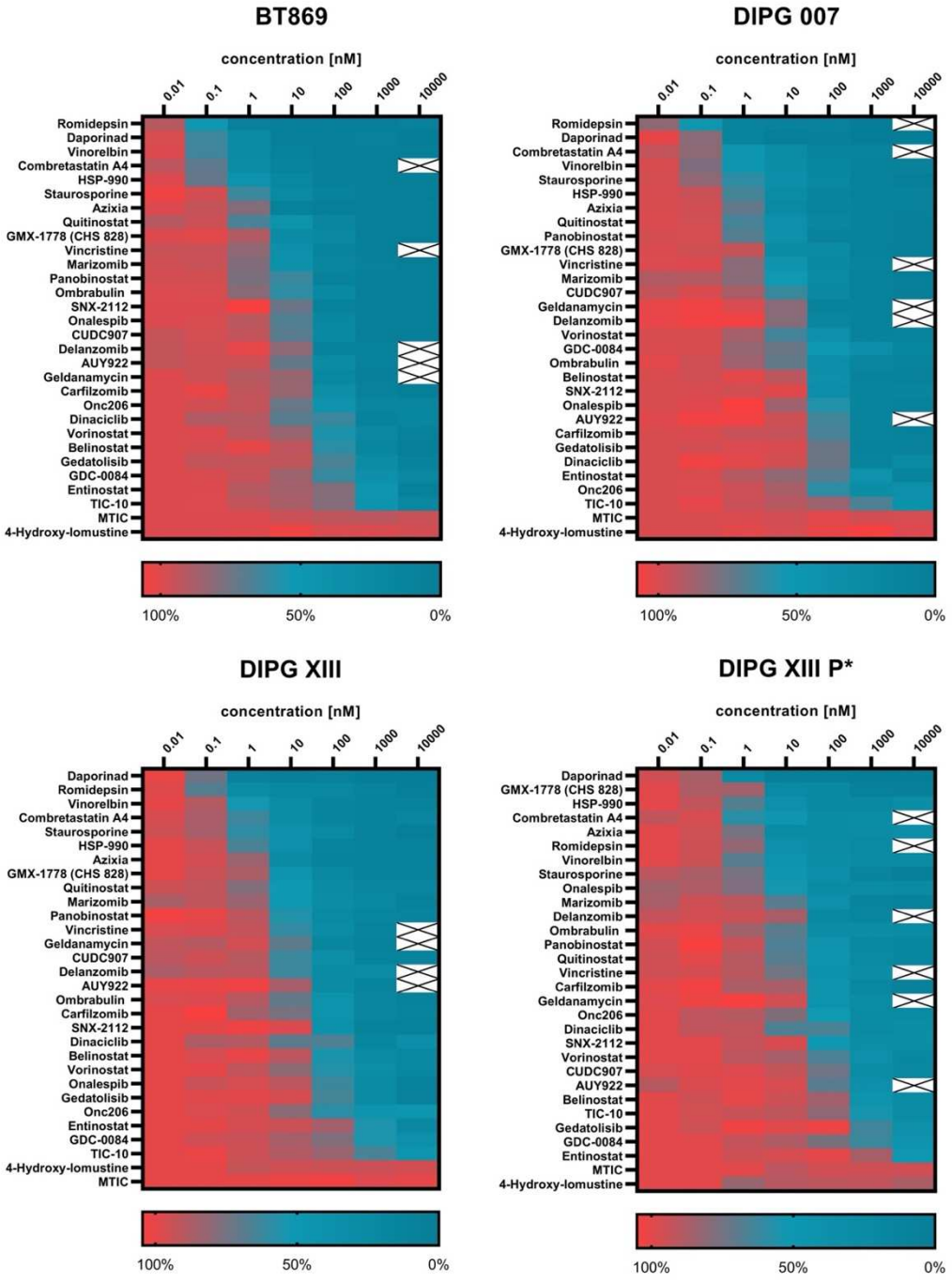

Figure 2: *In the above clustered heatmaps, each column represents a concentration in nanomolar, and each row indicates the viability of DMG tumor cells 72 hours after treatment with the chemotherapeutic agents in the left, normalized to the control (0,1%DMSO) and expressed as a percentage. All four DMG-cell lines are H3K27M-mutant with alteration in the histone variant H3.3.*

* The missing data points in the heatmaps (Fig. 1, Fig. 2) were not measured, either because the IC50 value could be determined from the slope of the dose-response curve with the existing data points, or because tumor cell viability was 0% at one-tenth of the non-measured concentration, which indisputably leads to complete tumor cell death at the non-measured concentration.

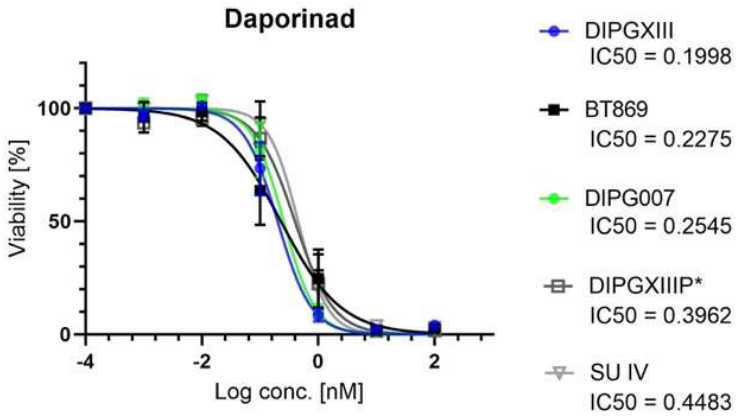

Figure 3: *Dose response curve of the NAMPT-Inhibitor daporinad. The IC50-values of Daporinad expressed in nanomolar are given for all five DMG-cell lines.*

The NAMPT inhibitor daporinad reduced the viability of DMG-tumor cells at concentrations lower than 1 nanomolar, indicating a high cytotoxic effect (Fig. 3). The other NAMPT inhibitor tested, GMX 1778, also showed low IC50 values, particularly in the more resistant cell line DIPG XIII P*, compared to the other agents (Fig. 2). Among the HDAC inhibitors, romidepsin and panobinostat had the lowest IC50 values (Figure 4), whereas belinostat, vorinostat, and entinostat reduced the DMG-cell viability at higher doses (IC50>0,1 µM) (Fig. 1, Fig. 2). The weakest antitumor cytotoxic effect of romidepsin is observed in the resistant DMG cell line DIPG XIIIP*, with an IC50 value more than twenty times higher than that of the other cell lines (Figure 4). This observation holds true for most of the drugs tested and is best illustrated in Fig. 2, but also in the dose-response curves of the individual chemotherapeutic agents, where the line representing DIPGXIIIP* lies above the lines of the other cell lines.

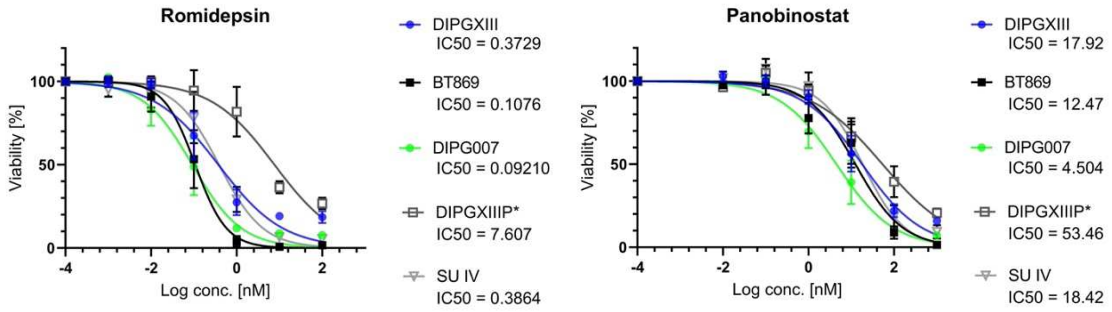

Figure 4: *Dose response curve of the HDAC-inhibitors panobinostat and romidepsin. The IC50-values expressed in nanomolar are given for all five DMG-cell lines.*

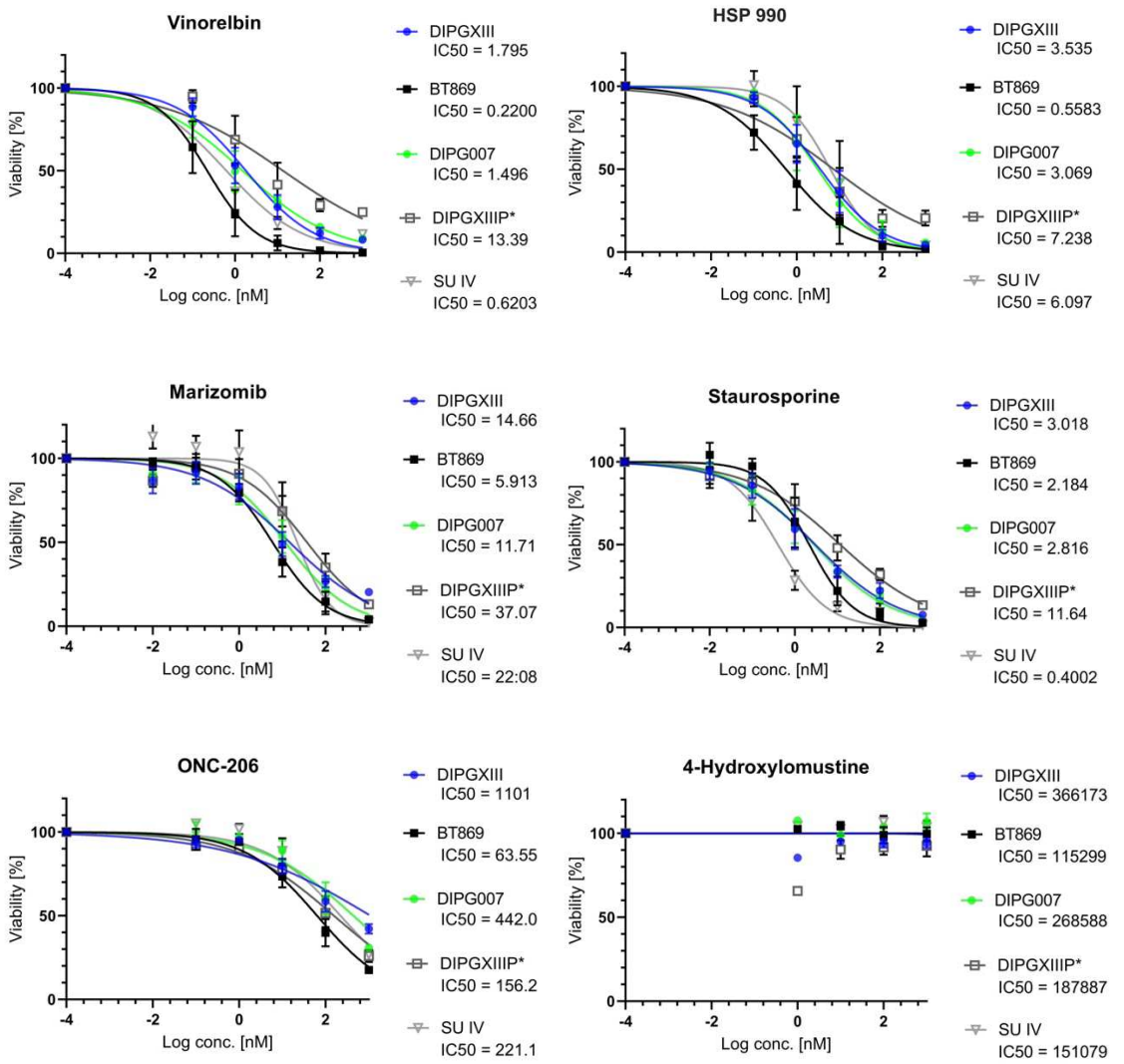

Figure 5: *Dose response curves of the vinca alkaloid vinorelbine, the HSP90 inhibitor HSP990, the pan-proteasome inhibitor marizomib, the multiple phosphokinase-inhibitor staurosporine, the dual DRD2 antagonist and ClpP agonist ONC206 and the alkylating agent 4-hydroxylomustine. The IC50-values of each agent expressed in nanomolar are given for all five DMG-cell lines.*

Among the microtubule-targeting agents vinorelbine, azixa and combrestastatin A4 had the lowest IC50 values for all cell lines, followed by vincristine and ombrabulin (Fig.2, Fig. 3, Fig. 5). The multiple phosphokinase inhibitor staurosporine (avg. IC50=4,01), the pan-proteasome inhibitor Marizomib (avg. IC50=18,29) and the HSP90-inhibitor HSP990 (avg. IC50=4,09), had the lowest IC50 values among drugs with the same mechanism of action in all cell lines. Dual DRD2 antagonist and ClpP agonists (ONC206, TIC10) and alkylating agents (4-hydroxylomustin and MTIC) had very high IC50 for DMG-tumor cells (Figure 5).

3.2 Potency ratio, a better predictor of anti-tumor activity than the IC50

In our *in vitro* IC50 assessment, it is possible to increase drug concentrations to levels far beyond what could be achieved *in vivo*. In fact, an important restriction in translating IC50 results from nonclinical experimental designs into clinical trials is the very use of concentrations far greater than those that could be realistically achieved in patients (54). To potentially obtain relevant clinical effects , the IC50 must be below the peak concentration (Cmax) - highest concentration reached in the bloodstream after systemic administration (55). Accordingly, we calculated the Cmax/IC50 ratio (potency ratio) with high therapeutic potential resulting in high potency ratios.

Table 3: *Logarithm of the calculated potency ratios (log10 [Cmax/IC50]). The Cmax values were gathered from the published clinical studies.*

		log10 [Cmax/IC50]				
		H3.3-mutation				H3.1-mutation
Drugs	**Cmax (nM)**	**DIPGXIII**	**BT869**	**DIPGXIIIP***	**DIPG007**	**SUIV**
Daporinad	14,1 (91)	1,8486	1,7922	1,7435	1,5513	1,4977
HSP 990	1307,3 (92)	2,5680	3,3695	2,6294	2,2568	2,3313
Romidepsin	1100 (93)	3,4698	4,0096	4,0771	2,1602	3,4544
Panobinostat	119 (94)	0,8222	0,9797	1,4219	0,3475	0,8103
Maizomib	191 (95)	1,1149	1,5092	1,2125	0,7120	0,9370
Staurosp.	65500 (96)	4,3365	4,4770	4,3666	3,7503	5,2140
Vincristine	28,4 (97)	0,0952	0,7042	0,4937	- 0,3867	0,4434
Vinorelbine	1856,8 (98)	3,0147	3,9263	3,0938	2,1420	3,4762
Lomustine	4707,1 (99)	- 1,8909	- 1,3891	- 1,7563	- 1,6012	- 1,5065
Azixa	1700,4(100)	2,6464	2,8951	2,7609	2,2844	3,1126
GMX-1778	839 (101)	2,0361	2,2619	2,1819	2,3228	2,2898
Quisinostat	7 (102)	- 0,2423	0,1971	0,2107	- 0,9682	- 0,2765
Geldanamyc.	10200 (103)	2,6764	2,4885	2,6370	1,9571	2,6928
CUDC907	22(104)	- 0,0942	- 0,0321	0,0605	- 1,2138	- 0,7404
Delanzomib	1139 (105)	1,5942	1,6673	1,5890	1,4799	1,6482
AUY922	2745,4(106)	1,8284	1,9708	1,3863	0,8861	1,8980
Ombrabulin	4900(107)	2,0213	2,5232	2,1061	2,0127	2,3007
Carfilzomib	1929,4(108)	1,5497	1,5836	1,0268	1,3713	1,3775
SNX-2112	2626,6(109)	1,5460	2,1269	1,5570	0,7836	1,7092
Onalespib	9254,7(110)	1,6614	2,6269	1,8300	1,6512	2,1455
Dinaciclib	4564,9(111)	1,4085	1,6780	1,2805	1,3761	0,9167
Belinostat	$4x10^4$(112)	2,3563	2,4260	2,7819	1,5784	2,1538
Vorinostat	2980(113)	1,1610	1,3455	1,9149	0,8740	0,9526
Gedatolisib	10651(114)	1,6799	1,6032	1,7005	0,5064	1,6331
Entinostat	303(115)	- 0,7498	- 0,3187	- 0,1145	- 1,7165	- 1,0595
MTIC	1962,4(116)	- 2,5860	- 2,5161	- 2,5264	- 2,2928	- 2,7255
Combrest. A4	1730(117)	2,8247	3,7374	3,0536	2,2759	2,6247

GDC0084	500(118)	-	0,6379	0,1807		0,6003	-	0,9476	- 0,8837
TIC 10	11125,8(119)		0,0123	1,2040		0,2944		0,7685	0,6401
ONC206	198	-	0,7451	0,4935	-	0,3488		0,1030	- 0,0479

A negative log potency ratio (log10 [Cmax/IC50]), i.e., a Cmax lower than the IC50, implies that the concentration required to kill 50% of DMG cells cannot be achieved in patients, making the drugs unsuitable for curative therapies. According to our data, the drugs on the far left of the graph have the best anti-tumor effect, with efficacy decreasing toward the right. The drugs marked in red have a Cmax that is lower than the IC50, indicating that their therapeutic concentration cannot be achieved in patients (Figure 6, Figure 7).

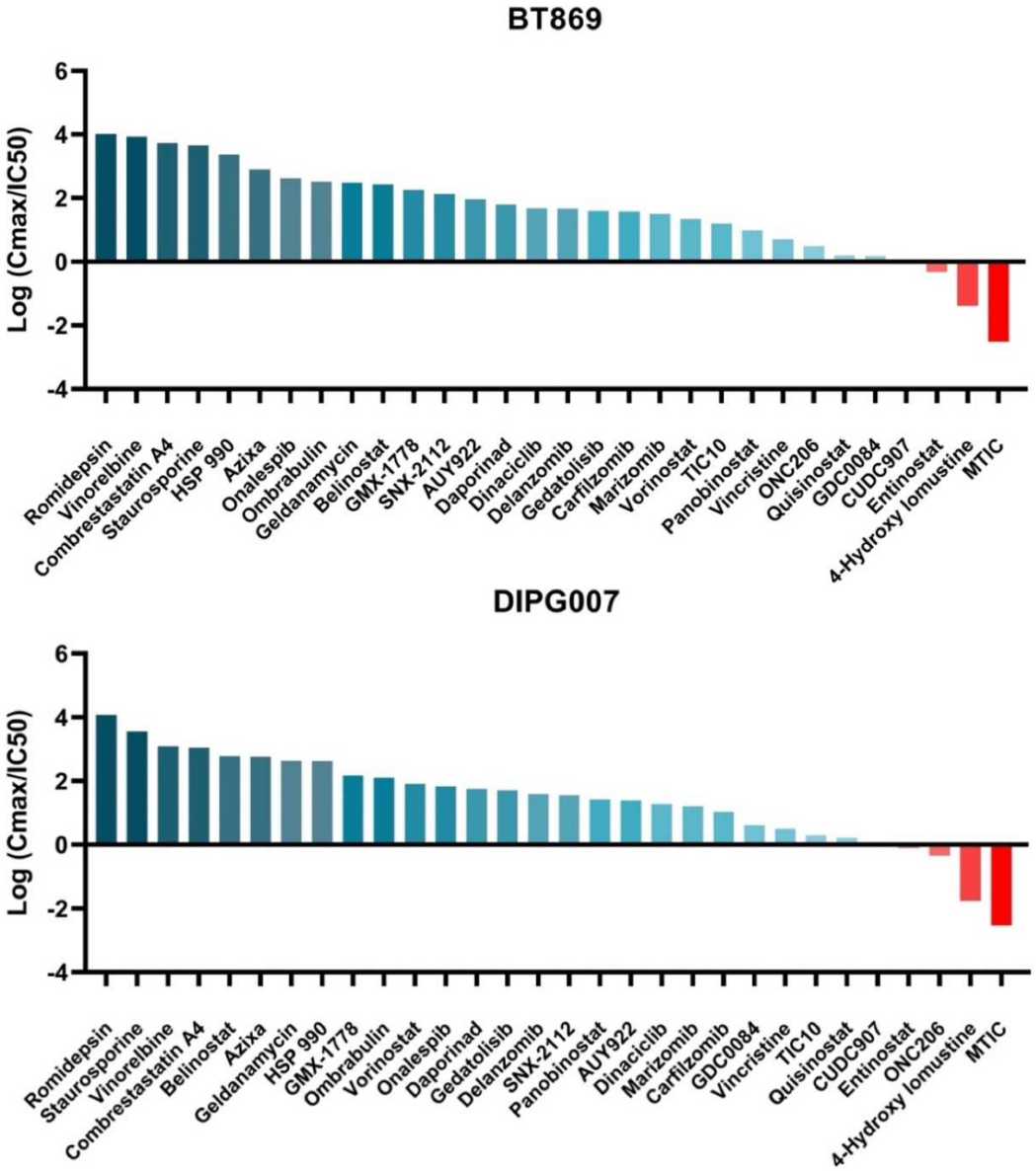

Figure 6: *Waterfall plot of logged potency ratios (log10 (Cmax/IC50)) for DMG cell lines BT869 and DIPG007, both harboring a K27M mutation in H3.3.*

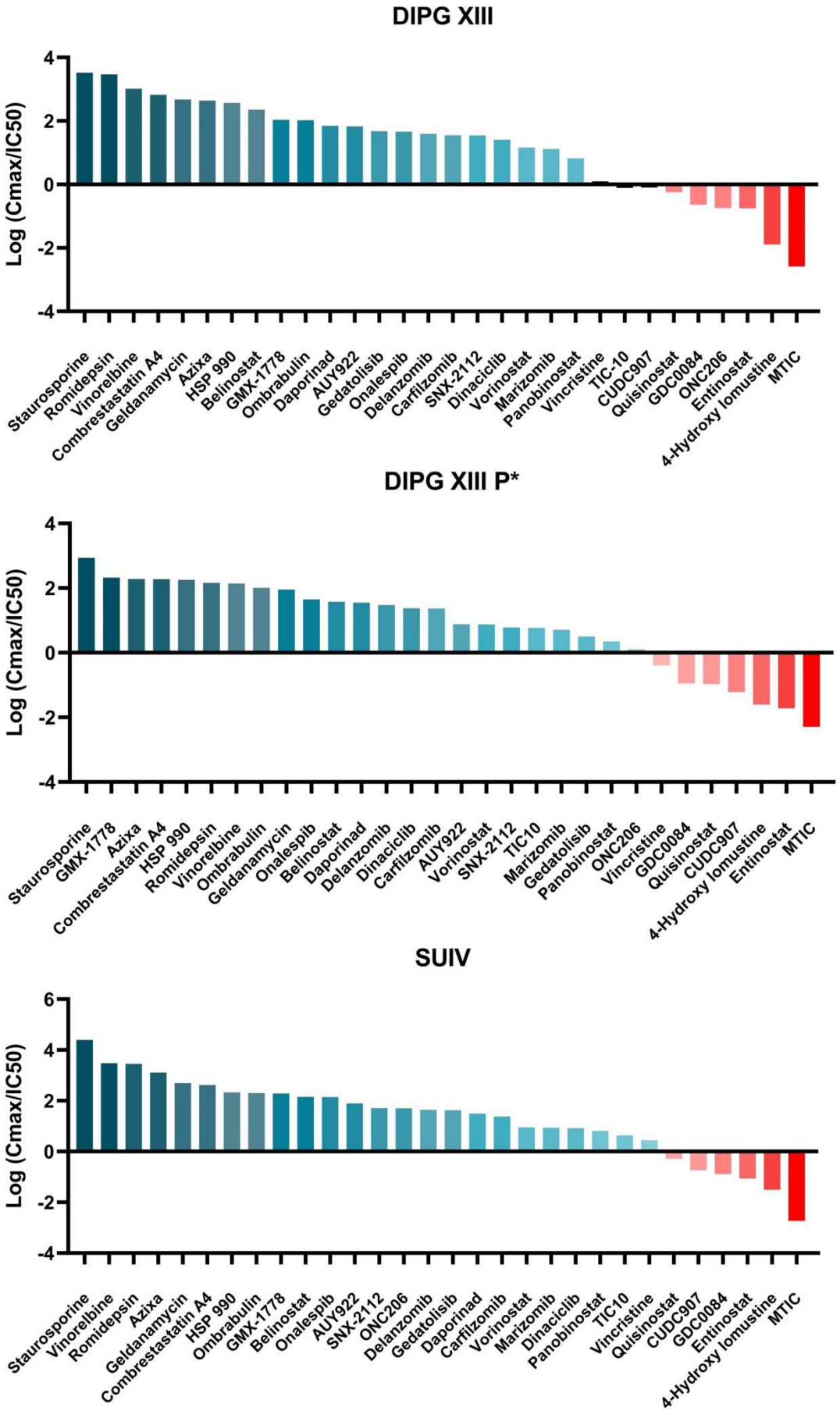

Figure 7: *Waterfall plot of logged potency ratios (log10 (Cmax/IC50)) for DMG cell lines DIPGXIII and DIPG XIIIP* harboring a K27M mutation in H3.3. and SUIV harboring a mutation in H3.1.*

3.3 Human iPSC- derived neuronal model for *in vitro* neurotoxicity assessment

3.3.1 Induction of neural stem cells from human derived iPSC line

The first step in generating various neural cells from iPSCs is the induction of iPSC to neural stem cells (NSCs) (67). IMR90-iPSCs maintained in feeder-free medium were differentiated in neural stem cell induction medium for 4 days after subculturing and further expanded in neuronal expansion medium for an additional 6 days in accordance with the protocol “Induction of Neural Stem Cells from Human Pluripotent Stem Cells” of Thermo Fischer Scientific (67). The generated neural progenitor cells were subsequently cryopreserved in STEMdiff Neural Progenitor Freezing and thawed for further testing when needed.

The differentiation of iPSC-derived NSCs was confirmed by expression of typical neural stem cell markers such as Nestin, Sox2 and PAX6 by immunocytochemistry (Fig. 8, Fig. 9). Additionally, NSCs exhibit a triangular to radial-like morphology forming networks through lengthening of the cellular process that differs from the flat round morphology of iPSCs that form compact colonies with well-defined borders (Figure 10).

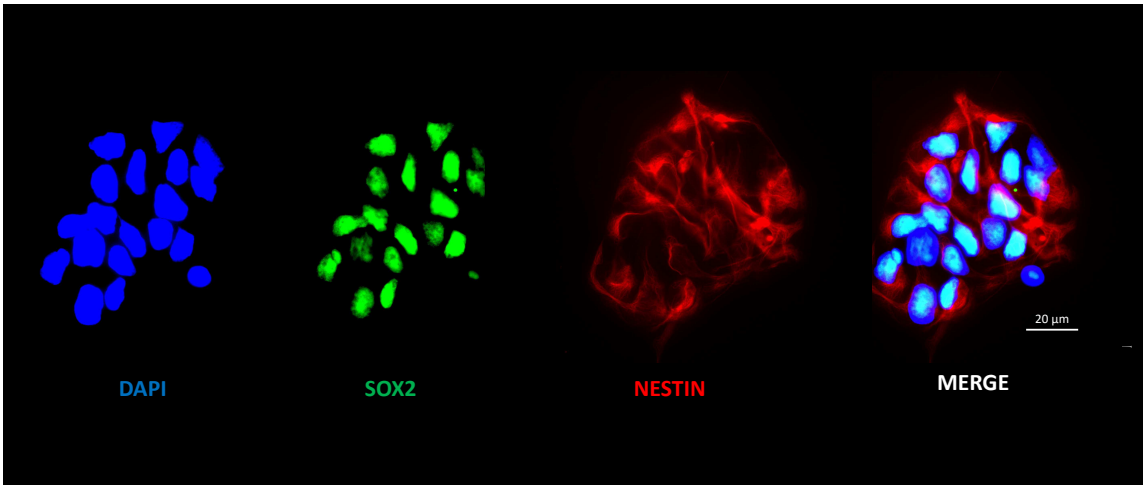

Figure 8: *Neural progenitor cells stained for sex-determining region Y - box 2 (SOX2; stem cell marker) and intermediate filament protein Nestin (neural stem/progenitor cell marker) with additional DAPI (nuclear DNA) staining. Scale bar depicts 20 µm.*

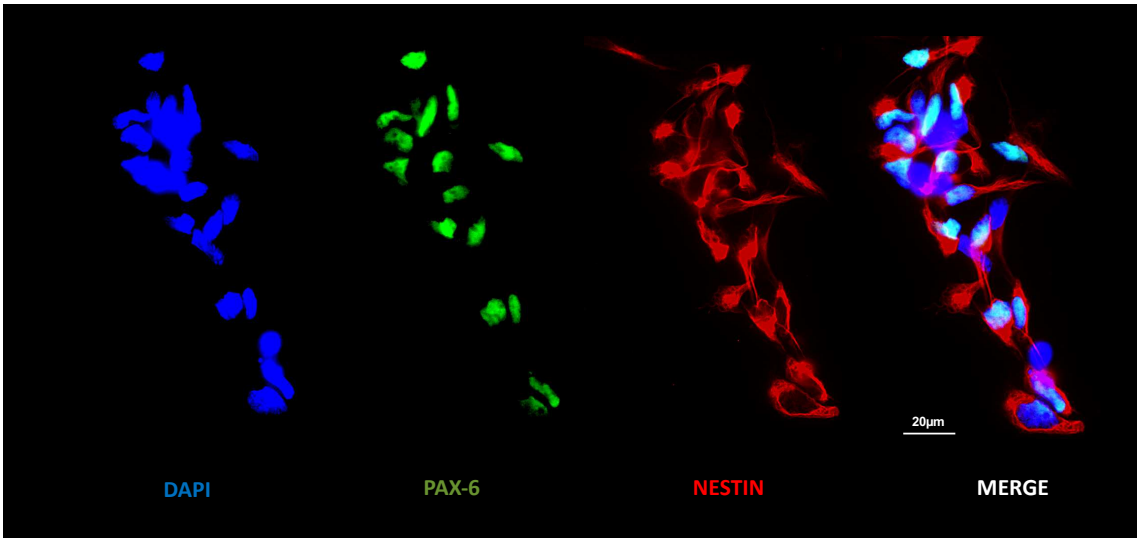

Figure 9: *Neural progenitor cells stained for Paired Box 6 (PAX6; stem cell marker) and intermediate filament protein Nestin (neural stem/progenitor cell marker) with additional DAPI (nuclear DNA) staining. Scale bar depicts 20 µm.*

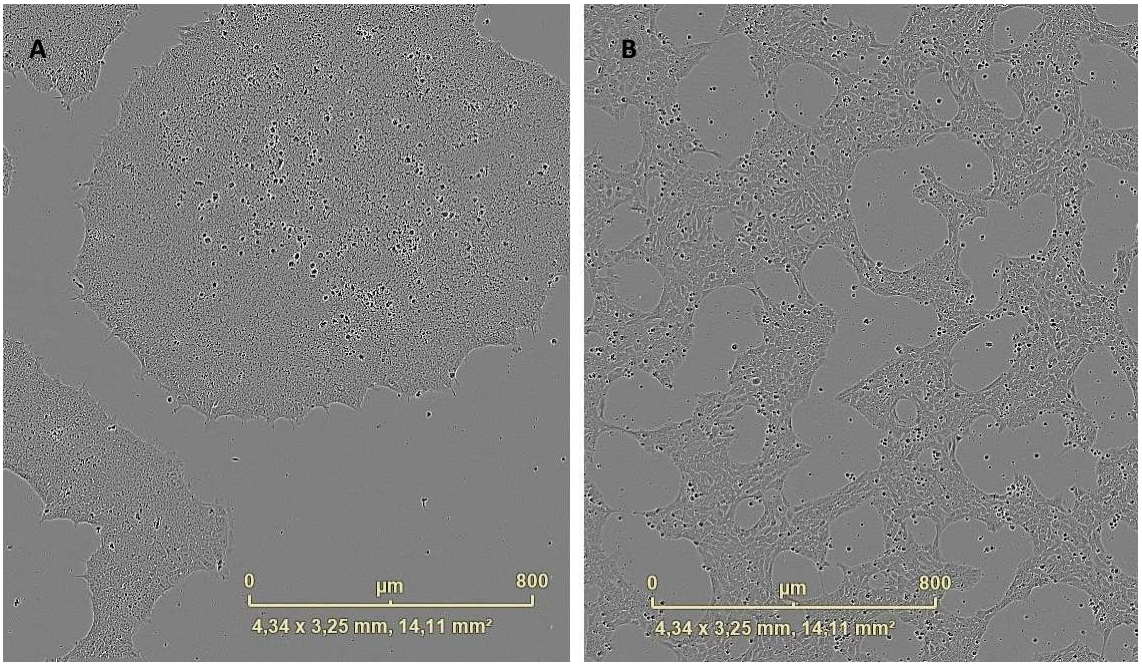

Figure 10: *(A) Phase contrast image of IMR90- iPSCs forming compact colonies with clearly defined borders. (B) Phase contrast image of triangular to radially shaped Neural Progenitor Cells (NPCs) forming networks through lengthening of the cellular process. (A, B) Scale bar depicts 800 µm.*

3.3.2 **Differentiation of neuronal network cultures**

NPCs were plated onto poly-L-ornithine/laminin-coated wells in neural expansion medium (day1) and then further induced in neural induction medium (neurobasal A medium and DMEM/F12 with glutamate, N2, B27-RA) supplemented with growth factors brain-derived neurotrophic factor (BDNF), glial cell-derived neurotrophic factor (GDNF), laminine, dibutyryl cyclic adenosine monophosphate and ascorbic acid. (120) Culture One Supplement was added into neuronal induction medium to prevent the overgrowth of contaminating progenitor cells while efficiently maintaining the population of neurons (69).

The derived cells were positive for the neuron-specific cytoskeletal marker β-III-tubulin (Tuj1) and dendritic marker MAP2, thus displaying important requisite markers for early neurons (Figure 11; Figure 12).

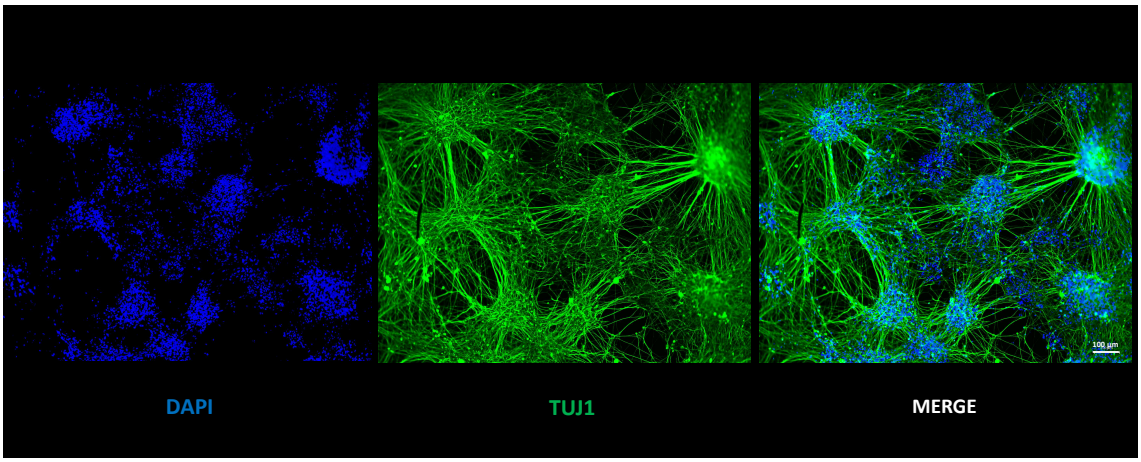

Figure 11: *Neural progenitor cells stained for anti-tubulin beta III isoform (Tuj1; early neuron marker) and DAPI (nuclear DNA). Scale bar depicts 100 µm.*

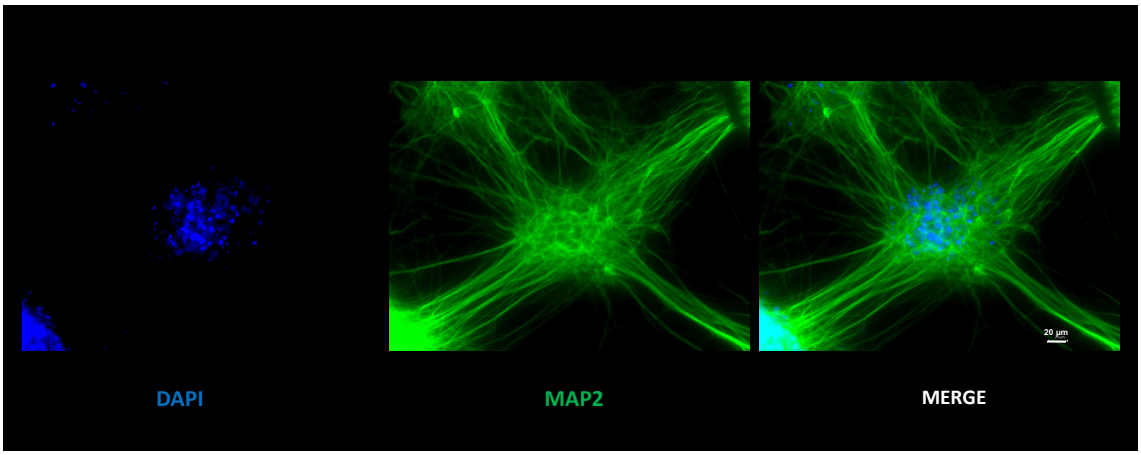

Figure 12: Neural progenitor cells stained for microtubule associated protein 2 (MAP2) and DAPI (nuclear DNA). Scale bar depicts 20 µm.

3.4 Neurotoxicity Assessment

Disruption of the synaptic function by natural or man- made neurotoxic substances or trauma can lead to long lasting and often irreversible effects and several studies suggest that neurites, as key features of the synapse and neural network formation, are sensible targets of chemical toxicity (69, 121, 122). Consequently, we used the neurite outgrowth per image area as test endpoint for our neurotoxicity assessment. Depending on the density, placement of neurons and the tendency to form neural cell body clusters, difficulties may arise when determining whether a particular neurite is coming from one neuronal cell body or the other (123). On that account the neurite outgrowth length was also normalized to cell body cluster area.

Experimental set-ups were carried out to determine the best media conditions and cell seeding density for developing early neurons from NPCs with the aim of increasing neurite growth per cell body cluster and reducing costs. Cells derived under the media conditions described previously (NPCs seeded in NEX and induced in NIM supplemented with BDNF and GDNF (refer to 3.2.2.)) were used as established controls to compare neurite length, branching, and morphology of the derived early neurons.

3.4.1 Neural expansion prior to neural induction increases neurite outgrowth

NPCs were plated onto poly-L-ornithine/laminin-coated 48-well plates. To determine the effect of expansion prior to induction, we plated half of the NPCs directly in NIM on day 1 of splitting and the other half in NEX (Fig. 13).

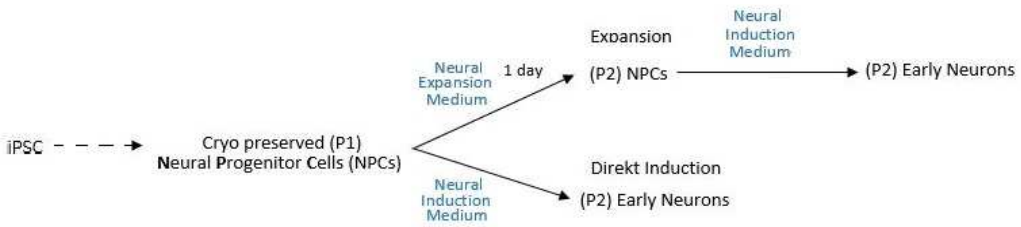

Figure 13: *Schematic illustration of the experimental set-up. Half of the NPCs were seeded on day 1 directly in NIM (Neural Induction Medium) and the other half in NEX (Neural Expansion Medium). From day 2 onwards, all NPCs were induced in NIM.*

From day two onwards, NPCs were induced in four Neural Induction Medium (NIM) compositions, each containing neurobasal A medium and DMEM/F12 with glutamate, N2, B27-RA supplemented with laminine, dibutyryl cyclic adenosine monophosphate, ascorbic acid and Culture One Supplement (abbreviated NIM--). The tested compositions of the Neural Induction Medium differ in the supplementation with the growth factors brain-derived neurotrophic factor (BDNF) and glia-cell-derived neurotrophic factor (GDNF), resulting in the following four compositions: NIM-BDNF, NIM-GDNF, NIM with both BDNF and GDNF (NIM++) and NIM without BDNF and GDNF (NIM--) (For each test condition we also seeded three different cell densities as follows: 30.000 cpw; 50.000 cpw and 70.000 cpw, respectively, 31579 cells / cm²; 52632 cells / cm² and 73684 cells / cm²). For each test condition we also seeded three different cell densities as follows: 30.000 cpw; 50.000 cpw and 70.000 cpw, respectively, 31579 cells / cm²; 52632 cells / cm² and 73684 cells / cm².

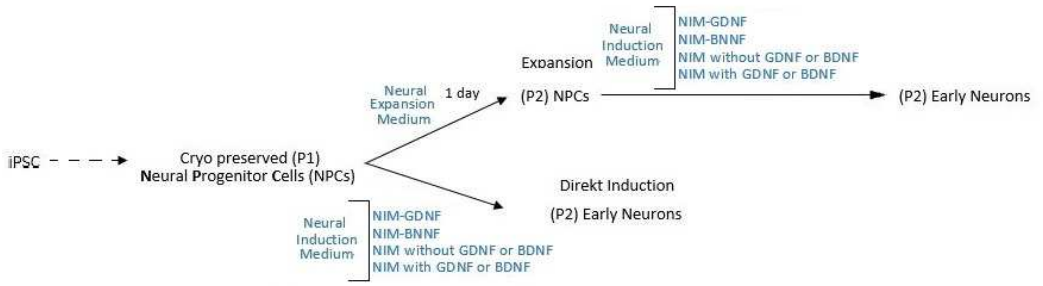

Figure 14: *Schematic illustration of the experimental set-up. NPCs were induced in four different medium compositions. For each of the testing condition three different cell densities were sown.*

The developing, label-free early neurons were imaged every three hours over the course of seven days by phase-contrast microscopy and the neurite length per image area expressed as mm/mm² image area and neurite length per cell-body cluster expressed as mm/mm² cell body cluster area were measured.

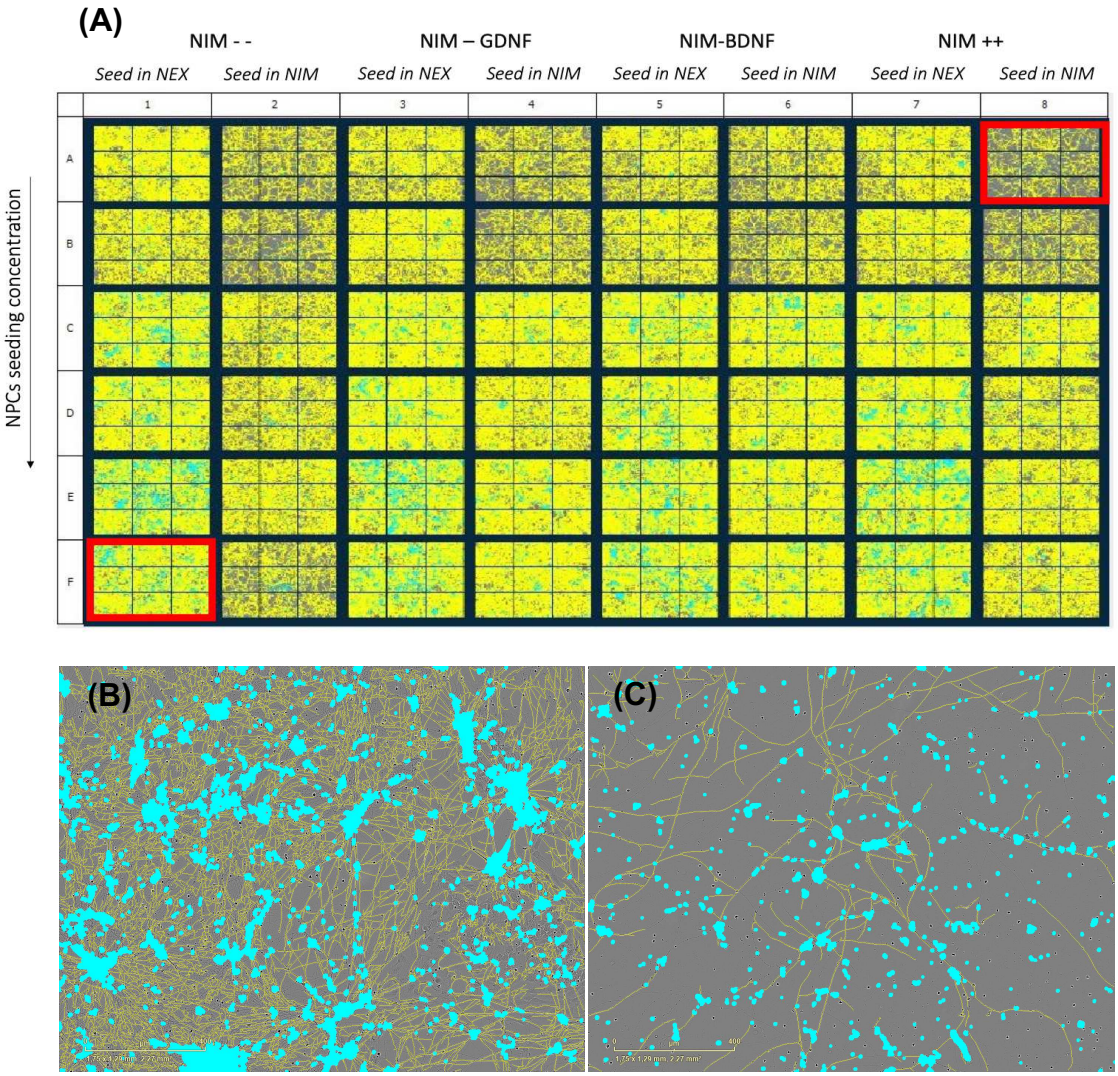

Figure 15: *Phase contrast images of neurites (yellow) and cell body clusters (blue) from iPSC-derived early neurons on day 7 of neural differentiation from NPCs.* ***(****A) Overview image of the early neurons when seeded under different NIM conditions and seeding concentrations. (B) Zoomed in section of the lower red box showing early neurons seeded in NIM-- at a density of 70.000 cpw. (C) Zoomed in section of the upper red box showing early neurons seeded in NIM++ at a density of 70.000 cpw. (A, B) Scale bar depicts 400 µm.*

Neural expansion in NEX prior to neural induction in NIM on day one of neural differentiation from frozen NPCs increases neurite length per image area regardless of the seeding density and the medium composition of NIM used from day 2 onwards (Figure 16).

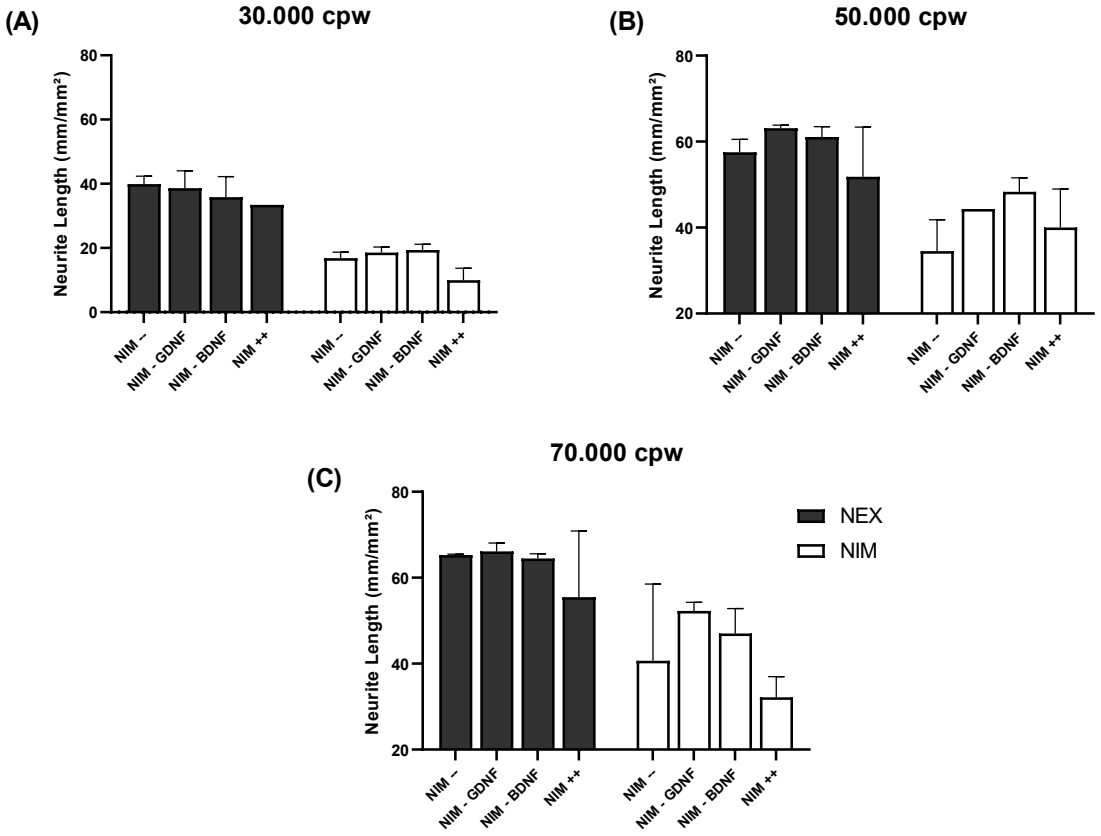

Figure 16: *Effects of Expansion in NEX prior to induction in NIM on day 1 of neural differentiation from frozen NPCs on the neurite length per image area (Mean ± SD). Neurite length was measured on day seven of the neural differentiation from NPCs in the different NIM medium compositions and expressed as mm/mm² image area. (A) Seeding density 30.000cpw (31.579 cells/cm²); (B) Seeding density 50.000 cpw (52.632 cells/cm²); (C) Seeding density 70.000cpw (73.684 cells/cm²).*

Our results indicated that neurite length per image area increases with higher seeding densities in all cells plated in NEX and differentiated in one of the NIM compositions. The difference in length of neurites per image area between the seeding density of 50.000 cpw and 70.000 cpw is negligible, compared to when 30.000 cpw and 50.000 cpw are seeded. Moreover, supplementation with BDNF and GDNF exerted only marginal effects on neurite outgrowth (Figure 16).

3.4.2 **A high degree of complexity and an overlap of neuronal outgrowths correlates with an increasing cell rate**

Considering the tendency of neuron bodies to cluster and thus overlap when forming higher order clusters (124) and the inability of 2D NeuroTrack analysis to identify neurites that grow on top of neuronal cell-bodies, we normalized the neurite length to body-cell cluster area.

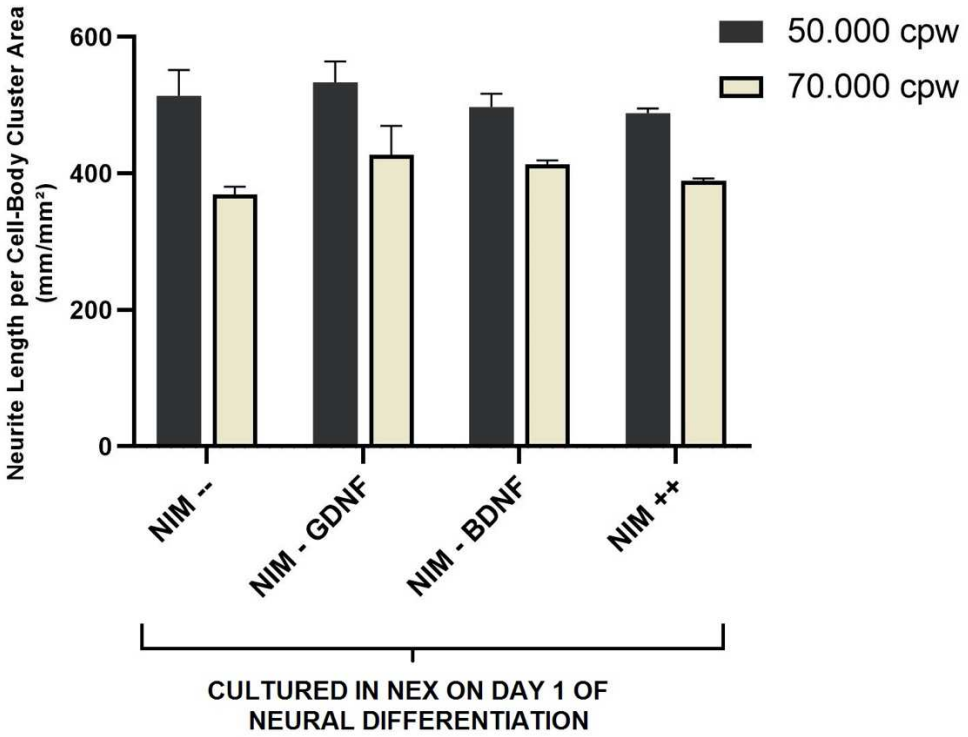

Figure 17: *Bar graph showing neurite length per cell-body cluster area (Mean ± SD) when NPCs were seeded in NEX and differentiated into one of the four NIM compositions at seeding densities of 50.000 cpw and 70.000 cpw. Neurite length per cell-body cluster area was measured on day seven of neural differentiation from NPCs and expressed as mm/mm² cell-body cluster area.*

Our results indicated that neurite length per cell-body cluster area is higher when 50.000 cpw were seeded in NEX, compared to 70.000 cpw, regardless of the NIM composition, in which NPCs were differentiated from day 2 onwards. Furthermore, supplementation with BDNF and GDNF exerted only marginal effects on neurite length per cell-body cluster area (Figure 17).

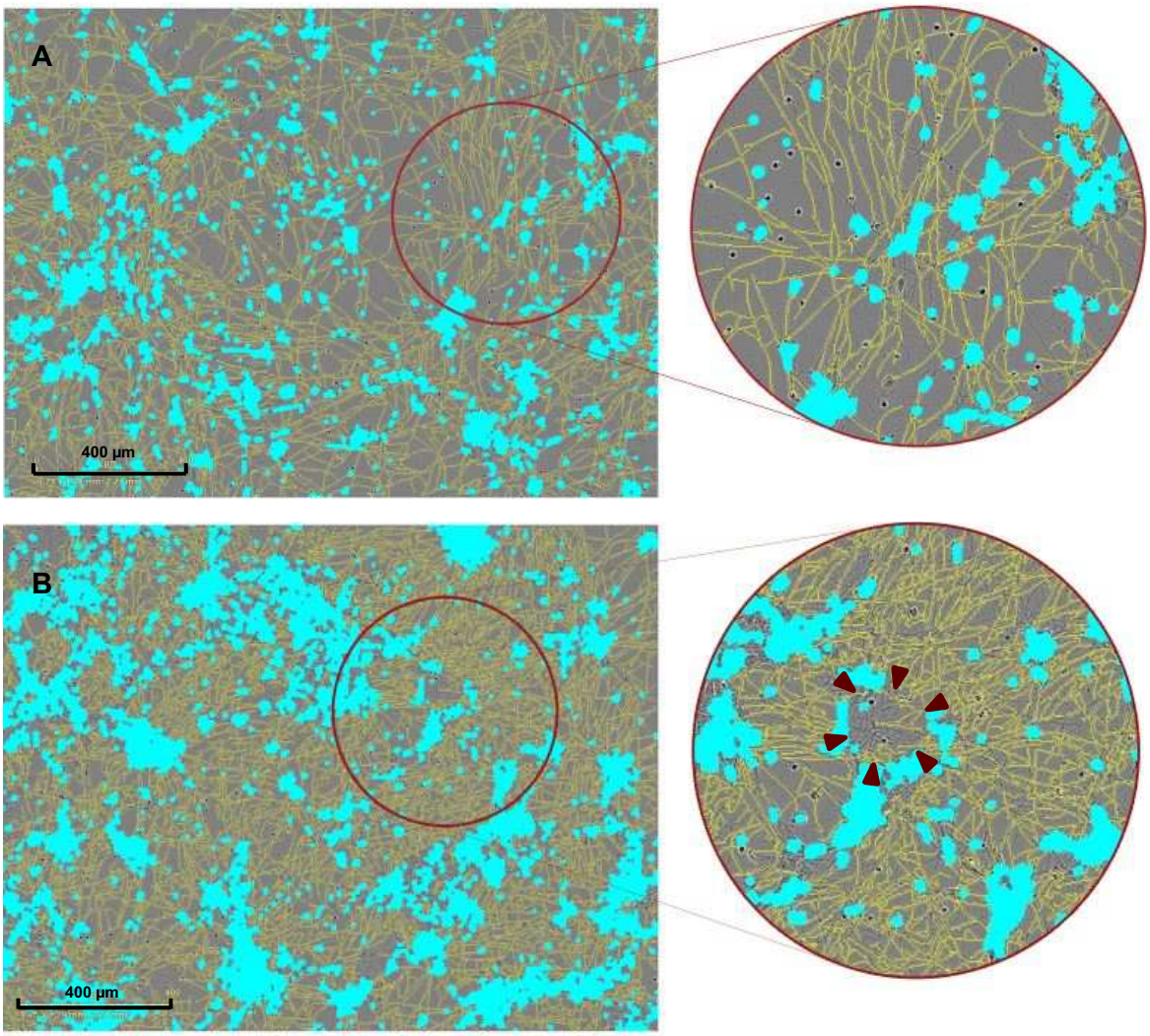

Figure 18: *Phase contrast images of neurites (yellow) and cell body clusters (blue) from iPSC-derived early neurons on day 7 of neural differentiation from NPCs. (A) Early neurons at a density of 50.000 cpw; (B) Early neurons at a density of 70.000 cpw; red arrows marking overlap of neuronal outgrowths not tracked from the analysis (A, B) Early neurons were differentiated from frozen NPCs, that were cultured in NEX on day 1 of differentiation and in NIM++ from day 2 onwards. Scale bar depicts 400 µm.*

At a density of 70.000 cpw, early neurons display a high degree of complexity and overlap of neuronal outgrowths, that cannot be recognized as such by the analysis (Figure 18).

3.4.3 **BDNF and GDNF supplementation does not affect contamination of neuronal cultures**

We looked for areas contaminated by non-neuronal cells / colonies to investigate the effect of brain-derived neurotrophic factor (BDNF) and glia-cell-derived neurotrophic factor (GDNF) on the purity of the early-neuron colonies. Irregularly distributed, non-neural colonies are found regardless of the supplementation with GDNF or BDNF (Figure 19).

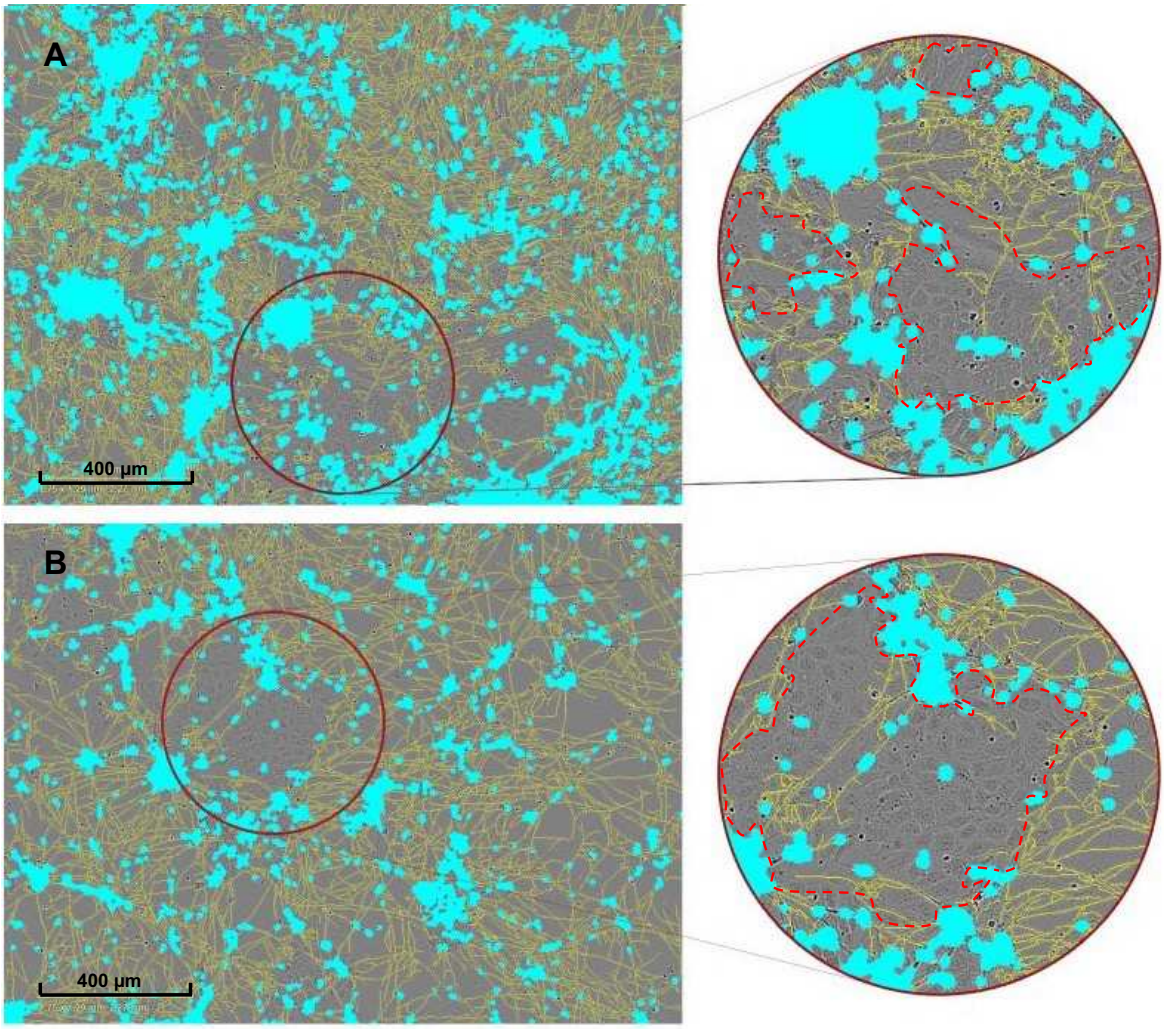

Figure 19: *Phase contrast images of neurites (yellow) and cell body clusters (blue) from iPSC-derived early neurons on day 7 of neural differentiation from NPCs. (A) Early neurons differentiated from frozen NPCs, that were cultured in NEX on day 1 of differentiation and in NIM-- from day 2 onwards; (B) Early neurons differentiated from frozen NPCs, that were cultured in NEX on day 1 of differentiation and in NIM++ from day 2 onwards.; (A; B) Areas circled in red mark non-neuronal differentiated colonies. Scale bar depicts 400 µm.*

3.4.4 **Assessment of drug-induced neurotoxicity**

Chemotherapy can have significant adverse effects on the central or peripheral nervous system, affecting the course of treatment. Recognition of drug-induced neurotoxicity is important to avoid neurological damage and to differentiate treatment-related symptoms from cancer progression into the nervous system (125). To assess drug-induced neurotoxicity of the chemotherapeutic agents in our panel, we conducted a label-free neurotoxicity assay, in which we evaluated the dynamic changes in neurite length of iPSC-derived neural cultures prior and after drug exposure over a 7-day period. The neurite length was compared to a DMSO-negative control, whereas as a positive control we used the validated neurotoxic agent Vincristine (126). 2D iPSC-derived neural cultures were exposed to two concentrations of each chemotherapeutic agent, the measured IC50 from the DMG cytotoxicity assessment and the researched cmax values from the literature. The neural cultures were imaged every 3 hours with the phase-contrast channel in the IncuCyte Live-Cell Analysis System.

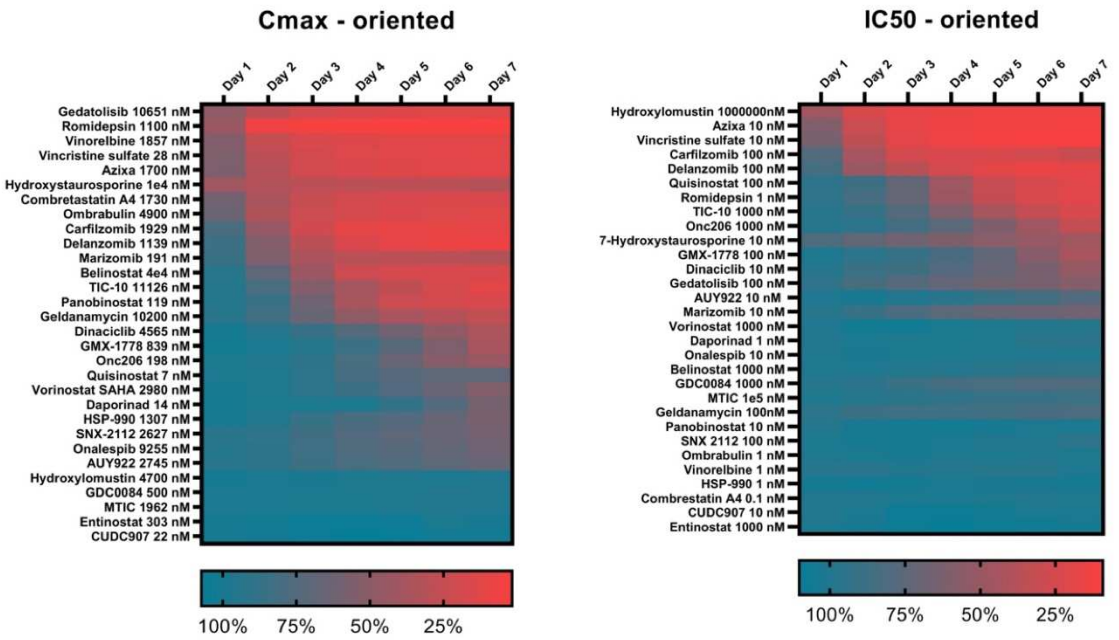

Figure 20: *In the above clustered heatmaps, each column represents a measurement time point and each row indicates the percentage of neurite length remaining after treatment with the chemotherapeutic agents at the given concentrations on the left compared to the negative control.*

Vincristine, a known neurotoxic agent, showed high neurotoxicity from a concentration of 10 nM in our assay. Other agents targeting microtubules, such as azixa, vinorelbine, combrestastatin A4, and ombrabulin, showed neurotoxic effects at theri Cmax concentrations. Notably, azixa is neurotoxic even at nanomolar concentration. The HDAC-Inhibitor Romidepsin is another agent with strong neurotoxic effects, reducing the neurite length notably from a concentration of 1 nM. The alkylating agents MTIC and hydroxylomustine don't affect the neurite length at their cmax concentration. For hydroxylomustine to exhibit neurotoxic effects, much higher concentrations are required than can realistically be achieved in patients. Carfilzomib, Delanzomib and Quisinostat reduce the neurite length notably from a concentration of 100nM. Most chemotherapeutic agents reduce neurite length prior to day 3 post-treatment. Some agents require longer exposure times (e.g., ONC206 at 1000 nM or GMX1778 at 100 nM).

4. Discussion

Diffuse midline glioma (DMG) has proven to be very challenging to treat. Numerous clinical trials with chemotherapeutic approaches have been conducted over the course of several decades in efforts to improve the outcome of DMG patients, none of which have shown promising therapeutic efficacy (127). The aim of this work is to identify novel therapeutic options for DMG using robust preclinical animal-free cell models. For this purpose, we assessed drug-cytotoxicity against DMG cells and drug-induced neurotoxicity of a group of thirty novel drugs, including five HSP90 inhibitors, five microtubule targeting agents, three proteasome inhibitors, two alkylating agents, two CDK-Inhibitors, two dual inhibitors of PI3K and mTOR, two NAMPT inhibitors, two dual DRD2 antagonist and ClpP agonist and seven HDAC inhibitors, one of which, CUCD 907, also acts as a PI3K inhibitor.

To evaluate drug-sensitivity of diffuse midline glioma, an *in vitro* cytotoxicity screen was performed on five patient-derived DMG cell lines, with half-maximal inhibitory concentration (IC50) as test endpoint. In our *in vitro* IC50 assessment, it is possible to increase drug concentrations to levels far beyond what could be achieved *in vivo*. In fact, an important limitation in implementing IC50 results from nonclinical experimental designs in clinical trials is the very use of concentrations far greater than those that could be realistically achieved in patients (54). To achieve therapeutic effects in the clinical setting, the IC50 should be below the peak concentration (Cmax) — the highest concentration reached in the bloodstream after systemic administration (55). For indicating the anti-tumor efficacy of the chemotherapeutic agents, we incorporated the *in vitro* measured IC50 data from our screening with the *in vivo* determined cmax data from the literature. Respectively, we calculated the Cmax/IC50 ratio (potency ratio), with high therapeutic potential leading to high potency ratios and vice versa.

Another recognized limitation of IC50 assessment is the considerably large data variability, that is highly protocol dependent (128). By keeping all test parameters (e.g., drug concentration and storage, treatment, and assay duration time, seeding density, medium composition, and volume) constant for all drugs, we tried to

minimize potential confounders and provided a more reliable comparison of the agents.

Furthermore, our simple single-agent DMG sensitivity assay, uses DMG suspension cells as targets. The simplicity of this cell culture brings fewer interfering factors, has high replicative potential, and is easy to maintain, but the cell-cell and cell-extracellular interactions are not as represented as they would be in the natural heterogeneous tumor mass. More complex models are needed to better mimic *in vivo* tumor tissue, such as iPSC-derived organoids or animal models.

A major obstacle between clinical application and tumor targets identification is the lack of efficient drug delivery across an intact BBB, limiting the central distribution of drugs that are beneficial to treat DMG (59, 60). BBB penetration depends on the expression of influx and efflux transporters and on the properties of the drug, requiring further more in-depth experiments (129). Furthermore, acquisition of drug resistance via altered mechanisms of cell biology is another complex challenge that is best addressed with combination therapy and warrants further investigation (62).

It is important to mention, that the IC50 values obtained in our *in vitro* drug response screening assay should only be used to compare the agents with each other and should not be extrapolated to IC50 values obtained in patients. Given the complexity of treating DMG, further, more in-depth drug validation experiments are needed to identify drugs that not only effectively target the tumor but also overcome obstacles in the clinical setting.

Drug safety issues remain a major source of attrition of clinical trials (56). In particular, neurotoxic side effects associated with chemotherapy administered during treatment can cause fatal damage with long-term disabling effects, limiting treatment options (57). Disruption of the synaptic function plays a major role in the associated neurotoxic side effects and studies suggest that neurites, as key features of the synapse and neural network formation, are sensible targets of chemical toxicity (69, 121, 122). In this thesis, we addressed the risk assessment of drug induced neurotoxicity of the selected therapeutic candidates and accordingly used the neurite length as test endpoint. Because conventional animal-

based toxicity assays are not only time-consuming, ethically controversial and expensinve, but also the results have limited translatability to humans, we used pluripotent stem cells (iPSCs) to induce human neurons, which we then used for neurotoxicity screening (130). Initial step in the generation of neural cells from iPSCs is the induction of iPSCs into neural stem cells (NSCs) (67). The differentiation of iPSC in NSCs was confirmed by expression of typical neural stem cell markers such as Nestin, Sox2 and PAX6 by immunocytochemistry. NPCs were subsequently differentiated into neuronal cultures, that were positive for the neuron-specific cytoskeletal marker β-III-tubulin (Tuj1) and dendritic marker MAP2, thus displaying important requisite markers for early neurons.

In our *in vitro* singe-agent screening, HSP90 inhibitors HSP990 and SNX2112 and NAMPT inhibitor daporinad were identified as promising anti-DMG candidates.

Based on our *in vitro* cytotoxicity data, HSP990 strongly reduced the DMG-cell viability at nanomolar concentrations (avg. IC50=4,1 nM) in all five DMG cell lines. The IC50 value lies far below the cmax value, suggesting that the drug concentration needed to reduce the DMG cell viability by 50% can be met in the bloodstream (avg. potency ratio=319). At the IC50 concentration, HSP90 exerted no effect on neurites, indicating that the drug has no neurotoxic side effects at this concentration. The moderate neurotoxic effect of HSP990 only at Cmax concentration and the high potency ratio suggests that HSP990 has a wide therapeutic window. Altogether, our data indicates that HSP990 is a potential novel agent against DMG.

NAMPT inhibitor daporinad also strongly reduced the DMG-cell viability at very low concentrations (avg. IC50=0,3 nM) in all five DMG cell lines and demonstrated a high potency ratio of 46,2. Daporinad exerted no effect on neurites at the IC50 concentration. At the cmax concentration of 14 nM, daporinad reduced the neurite length of iPSC-derived neuronal cultures by 12 % over a seven-day period, suggesting for a moderate neurotoxic side effect.

The IC50 values of HSP90 inhibitor SNX2112 showed considerable variability between the different DMG cell lines. The cell line BT869 was the most sensitive to SNX2112 (IC50=19,6 nM), while DIPGXIIIP* was the most resistant

(IC50=432,3 nM). On average, the potency ratio was high at 52.5. Discrepancies in IC50 among the DMG cell lines suggest that more personalized therapies are required for optimal management of DMG in the future. In addition, SNX2112 showed no neurotoxic effect at its IC50 concentration, yet a 20% decrease in neurite length at its cmax concentration over a seven-day period and therefore should be administered with caution due to its neurotoxic side effects. Altogether, SNX2112 is a potential novel therapeutic approach against DMG, that should be carefully monitored for its dose-dependent neurotoxic effects.

Our screen indicated high *in vitro* DMG cytotoxicity at nanomolar concentrations for combretastatin, and Vinorelbin (avg. Combrestastatin A4-IC50=3.5 nM; avg. Vinorelbin-IC50=3.5 nM) in all five DMG cell lines. IC50 values are also well below cmax for both agents. At their IC50 concentration, neither drug damages neurites, but at their cmax concentration, they show remarkable neurotoxicity by dramatically reducing neurite length by 80% (vinorelbine) and 74% (combrestastatin) over a seven-day period. Taken together, vinorelbine and combrestatine may be potential targets of DMG, but their administration should be closely monitored because of their dose-dependent neurotoxic side effects. Similarly, geldanamycin and belinostat showed good potency ratios across all cell lines and only mild neurotoxic effects at the IC50 concentration, reducing neurite length by 7% (geldanamycinn) and 3% (belinostat), but a very notable neurotoxic effect at cmax concentration, reducing neurite length to 51% (geldanamycin) and to 39% (belinostat) over a seven-day period.

This screen also revealed high in vitro DMG cytotoxicity for HDAC inhibitor Romidepsin, with IC50 values more than 650-fold below Cmax, suggesting that romidepsin has high anti-tumor potential. Nevertheless, at the cmax concentration of 1100 nM, romidepsin drastically reduced the neurite length of iPSC-derived neuronal cultures by 76 % over a seven-day period. Indeed, even at 1nM, neurite length was reduced to 53% over the course of seven days, suggesting that romidepsin has a very narrow therapeutic window. Similarly, staurosporine, azixa GMX-1778, AUY922 and Carfilzomib have good potency ratios, yet show high neurotoxicity from even IC50 levels.

The HDAC inhibitor panobinostat showed a moderate potency against DMG cells (avg. IC50=21,4nM) with variability between the different DMG cell lines. The cell line DIPG007 was the most sensitive to panobinostat (IC50=4,5 nM), while DIPGXIIIP* was the most resistant (IC50=53,5 nM). On average, the potency ratio was 10,3. Furthermore, Panobinostat showed no neurotoxic effect at 10 nM, yet a 53% decrease in neurite length at its cmax concentration of only 119 nM over a seven-day period.

The alkylating agents MTIC and 4-hydroxylomustine along with the HDAC inhibitors entinostat and CUDC907 have IC50 values well above cmax in all DMG cell lines, meaning that the concentration required to kill 50% of DMG cells cannot be achieved in patients, making the drugs unsuitable for curative therapies. None of the four drugs had any impact on neurites at their Cmax concentrations, suggesting that they are not neurotoxic in patients. At the IC50 concentration of 4-hydroxylomustine (IC50=1M), which is unattainable in the clinical setting, all neurites were damaged. Potency ratios of quisinostat, GDC0084 are also very poor for all DMG cell lines. (Cmax/IC50~0). These drugs showed very low neurotoxicity in our assay at their Cmax concentrations, implying that they exhibit negligible neurotoxicity in patients. Although these drugs are ineffective in treating diffuse midline glioma because their antitumor potency against DMG is not sufficiently high, knowledge of their neurotoxic side effects are important for safe administration to patients in other diseases.

In contrast, vincristine and TIC10, which are also poorly effective against all DMG cell lines (Cmax/IC50~0), show high neurotoxicity at their cmax concentration. Thus, they are not only unsuitable as treatment against DMG, but should also be administered only with great caution in other conditions because of their neurotoxic side effects.

5. Conclusion

Diffuse midline glioma (DMG) has proven very challenging to treat. In this thesis we performed a single-agent sensitivity drug screen against DMG and a neurotoxicity assessment of thirty novel chemotherapeutic agents to search for promising novel therapies and provide a basis for planning clinical trials. In our screen, HSP90 inhibitors HSP990 and SNX2112 and NAMPT inhibitor daporinad were identified as promising anti-DMG candidates with a wide therapeutic window. IC50 discrepancies among cell lines indicate different sensitivity to various chemotherapeutic agents, warranting for more personalized therapies in the future.

Our *in vitro* drug screening provides insights into neurotoxicity and efficacy against various DMG cell lines but does not account for other treatment challenges such as BBB penetration, drug resistance, and cell-environment interaction. Given the complexity of treating DMG, further, more in-depth drug validation experiments are needed.

References

1. Howlader N NA, Krapcho M, Miller D, Brest A, Yu M, Ruhl J, Tatalovich Z, Mariotto A, Lewis DR, Chen HS, Feuer EJ, Cronin KA (eds). . SEER Cancer Statistics Review, 1975-2018, National Cancer Institute. Bethesda, MD, https://seer.cancer.gov/csr/1975_2018/, based on November 2020 SEER data submission, posted to the SEER web site, April 2021.

2. de Blank PM, Ostrom QT, Rouse C, Wolinsky Y, Kruchko C, Salcido J, et al. Years of life lived with disease and years of potential life lost in children who die of cancer in the United States, 2009. Cancer Med. 2015;4(4):608-19.

3. Hargrave D, Bartels U, Bouffet E. Diffuse brainstem glioma in children: critical review of clinical trials. Lancet Oncol. 2006;7(3):241-8.

4. Jones C, Perryman L, Hargrave D. Paediatric and adult malignant glioma: close relatives or distant cousins? Nat Rev Clin Oncol. 2012;9(7):400-13.

5. Louis DN, Perry A, Wesseling P, Brat DJ, Cree IA, Figarella-Branger D, et al. The 2021 WHO Classification of Tumors of the Central Nervous System: a summary. Neuro Oncol. 2021;23(8):1231-51.

6. Wu G, Broniscer A, McEachron TA, Lu C, Paugh BS, Becksfort J, et al. Somatic histone H3 alterations in pediatric diffuse intrinsic pontine gliomas and non-brainstem glioblastomas. Nat Genet. 2012;44(3):251-3.

7. Khuong-Quang DA, Buczkowicz P, Rakopoulos P, Liu XY, Fontebasso AM, Bouffet E, et al. K27M mutation in histone H3.3 defines clinically and biologically distinct subgroups of pediatric diffuse intrinsic pontine gliomas. Acta Neuropathol. 2012;124(3):439-47.

8. Srikanthan D, Taccone MS, Van Ommeren R, Ishida J, Krumholtz SL, Rutka JT. Diffuse intrinsic pontine glioma: current insights and future directions. Chin Neurosurg J. 2021;7(1):6.

9. Schroeder KM, Hoeman CM, Becher OJ. Children are not just little adults: recent advances in understanding of diffuse intrinsic pontine glioma biology. Pediatr Res. 2014;75(1-2):205-9.

10. Sarma A, Heck JM, Bhatia A, Krishnasarma RS, Pruthi S. Magnetic resonance imaging of the brainstem in children, part 2: acquired pathology of the pediatric brainstem. Pediatr Radiol. 2021;51(2):189-204.

11. Buczkowicz P, Bartels U, Bouffet E, Becher O, Hawkins C. Histopathological spectrum of paediatric diffuse intrinsic pontine glioma: diagnostic and therapeutic implications. Acta Neuropathol. 2014;128(4):573-81.

12. Albright AL, Packer RJ, Zimmerman R, Rorke LB, Boyett J, Hammond GD. Magnetic resonance scans should replace biopsies for the diagnosis of diffuse brain stem gliomas: a report from the Children's Cancer Group. Neurosurgery. 1993;33(6):1026-9; discussion 9-30.

13. Johnson KJ, Cullen J, Barnholtz-Sloan JS, Ostrom QT, Langer CE, Turner MC, et al. Childhood brain tumor epidemiology: a brain tumor epidemiology consortium review. Cancer Epidemiol Biomarkers Prev. 2014;23(12):2716-36.

14. Johung TB, Monje M. Diffuse Intrinsic Pontine Glioma: New Pathophysiological Insights and Emerging Therapeutic Targets. Curr Neuropharmacol. 2017;15(1):88-97.

15. Walker DA, Liu J, Kieran M, Jabado N, Picton S, Packer R, et al. A multi-disciplinary consensus statement concerning surgical approaches to low-grade, high-grade astrocytomas and diffuse intrinsic pontine gliomas in childhood (CPN Paris 2011) using the Delphi method. Neuro Oncol. 2013;15(4):462-8.

16. Schumacher M, Schulte-Monting J, Stoeter P, Warmuth-Metz M, Solymosi L. Magnetic resonance imaging compared with biopsy in the diagnosis of brainstem diseases of childhood: a multicenter review. J Neurosurg. 2007;106(2 Suppl):111-9.

17. Friedrich C, Warmuth-Metz M, von Bueren AO, Nowak J, Bison B, von Hoff K, et al. Primitive neuroectodermal tumors of the brainstem in children treated according to the HIT trials: clinical findings of a rare disease. J Neurosurg Pediatr. 2015;15(3):227-35.

18. J. D. Diffuse midline glioma, H3 K27M mutant. PathologyOutlines.com website. https://wwwpathologyoutlinescom/topic/cnstumordmgh3k27mhtml Accessed July 27th, 2021.

19. Albright AL, Guthkelch AN, Packer RJ, Price RA, Rourke LB. Prognostic factors in pediatric brain-stem gliomas. J Neurosurg. 1986;65(6):751-5.

20. Fisher PG, Breiter SN, Carson BS, Wharam MD, Williams JA, Weingart JD, et al. A clinicopathologic reappraisal of brain stem tumor classification. Identification of pilocystic astrocytoma and fibrillary astrocytoma as distinct entities. Cancer. 2000;89(7):1569-76.

21. Yoshimura J, Onda K, Tanaka R, Takahashi H. Clinicopathological study of diffuse type brainstem gliomas: analysis of 40 autopsy cases. Neurol Med Chir (Tokyo). 2003;43(8):375-82; discussion 82.

22. Leach JL, Roebker J, Schafer A, Baugh J, Chaney B, Fuller C, et al. MR imaging features of diffuse intrinsic pontine glioma and relationship to overall survival: report from the International DIPG Registry. Neuro Oncol. 2020;22(11):1647-57.

23. Aboian MS, Solomon DA, Felton E, Mabray MC, Villanueva-Meyer JE, Mueller S, et al. Imaging Characteristics of Pediatric Diffuse Midline Gliomas with Histone H3 K27M Mutation. AJNR Am J Neuroradiol. 2017;38(4):795-800.

24. Li Q, Dong F, Jiang B, Zhang M. Exploring MRI Characteristics of Brain Diffuse Midline Gliomas With the H3 K27M Mutation Using Radiomics. Front Oncol. 2021;11:646267.

25. Calmon R, Puget S, Varlet P, Beccaria K, Blauwblomme T, Grevent D, et al. Multimodal Magnetic Resonance Imaging of Treatment-Induced Changes to Diffuse Infiltrating Pontine Gliomas in Children and Correlation to Patient Progression-Free Survival. Int J Radiat Oncol Biol Phys. 2017;99(2):476-85.

26. Szychot E, Youssef A, Ganeshan B, Endozo R, Hyare H, Gains J, et al. Predicting outcome in childhood diffuse midline gliomas using magnetic resonance imaging based texture analysis. J Neuroradiol. 2021;48(4):243-7.

27. Castel D, Philippe C, Calmon R, Le Dret L, Truffaux N, Boddaert N, et al. Histone H3F3A and HIST1H3B K27M mutations define two subgroups of diffuse intrinsic pontine gliomas with different prognosis and phenotypes. Acta Neuropathol. 2015;130(6):815-27.

28. Chan KM, Fang D, Gan H, Hashizume R, Yu C, Schroeder M, et al. The histone H3.3K27M mutation in pediatric glioma reprograms H3K27 methylation and gene expression. Genes Dev. 2013;27(9):985-90.

29. Fang D, Gan H, Cheng L, Lee JH, Zhou H, Sarkaria JN, et al. H3.3K27M mutant proteins reprogram epigenome by sequestering the PRC2 complex to poised enhancers. Elife. 2018;7.

30. Paugh BS, Broniscer A, Qu C, Miller CP, Zhang J, Tatevossian RG, et al. Genome-wide analyses identify recurrent amplifications of receptor tyrosine kinases and cell-cycle regulatory genes in diffuse intrinsic pontine glioma. J Clin Oncol. 2011;29(30):3999-4006.

31. Paugh BS, Zhu X, Qu C, Endersby R, Diaz AK, Zhang J, et al. Novel oncogenic PDGFRA mutations in pediatric high-grade gliomas. Cancer Res. 2013;73(20):6219-29.

32. Puget S, Philippe C, Bax DA, Job B, Varlet P, Junier MP, et al. Mesenchymal transition and PDGFRA amplification/mutation are key distinct oncogenic events in pediatric diffuse intrinsic pontine gliomas. PLoS One. 2012;7(2):e30313.

33. Grill J, Puget S, Andreiuolo F, Philippe C, MacConaill L, Kieran MW. Critical oncogenic mutations in newly diagnosed pediatric diffuse intrinsic pontine glioma. Pediatr Blood Cancer. 2012;58(4):489-91.

34. Zarghooni M, Bartels U, Lee E, Buczkowicz P, Morrison A, Huang A, et al. Whole-genome profiling of pediatric diffuse intrinsic pontine gliomas highlights platelet-derived growth factor receptor alpha and poly (ADP-ribose) polymerase as potential therapeutic targets. J Clin Oncol. 2010;28(8):1337-44.

35. Wu G, Diaz AK, Paugh BS, Rankin SL, Ju B, Li Y, et al. The genomic landscape of diffuse intrinsic pontine glioma and pediatric non-brainstem high-grade glioma. Nat Genet. 2014;46(5):444-50.

36. Gururangan S, McLaughlin CA, Brashears J, Watral MA, Provenzale J, Coleman RE, et al. Incidence and patterns of neuraxis metastases in children with diffuse pontine glioma. J Neurooncol. 2006;77(2):207-12.

37. Halperin EC. Pediatric brain stem tumors: patterns of treatment failure and their implications for radiotherapy. Int J Radiat Oncol Biol Phys. 1985;11(7):1293-8.

38. Vanan MI, Eisenstat DD. DIPG in Children - What Can We Learn from the Past? Front Oncol. 2015;5:237.

39. Frazier JL, Lee J, Thomale UW, Noggle JC, Cohen KJ, Jallo GI. Treatment of diffuse intrinsic brainstem gliomas: failed approaches and future strategies. J Neurosurg Pediatr. 2009;3(4):259-69.

40. Meel MH, Kaspers GJL, Hulleman E. Preclinical therapeutic targets in diffuse midline glioma. Drug Resist Updat. 2019;44:15-25.

41. Grasso CS, Tang Y, Truffaux N, Berlow NE, Liu L, Debily MA, et al. Functionally defined therapeutic targets in diffuse intrinsic pontine glioma. Nat Med. 2015;21(6):555-9.

42. Piunti A, Hashizume R, Morgan MA, Bartom ET, Horbinski CM, Marshall SA, et al. Therapeutic targeting of polycomb and BET bromodomain proteins in diffuse intrinsic pontine gliomas. Nat Med. 2017;23(4):493-500.

43. Hashizume R, Andor N, Ihara Y, Lerner R, Gan H, Chen X, et al. Pharmacologic inhibition of histone demethylation as a therapy for pediatric brainstem glioma. Nat Med. 2014;20(12):1394-6.

44. Hennika T, Hu G, Olaciregui NG, Barton KL, Ehteda A, Chitranjan A, et al. Pre-Clinical Study of Panobinostat in Xenograft and Genetically Engineered Murine Diffuse Intrinsic Pontine Glioma Models. PLoS One. 2017;12(1):e0169485.

45. Mohammad F, Weissmann S, Leblanc B, Pandey DP, Hojfeldt JW, Comet I, et al. EZH2 is a potential therapeutic target for H3K27M-mutant pediatric gliomas. Nat Med. 2017;23(4):483-92.

46. Wiese M, Schill F, Sturm D, Pfister S, Hulleman E, Johnsen SA, et al. No Significant Cytotoxic Effect of the EZH2 Inhibitor Tazemetostat (EPZ-6438) on Pediatric Glioma Cells with Wildtype Histone 3 or Mutated Histone 3.3. Klin Padiatr. 2016;228(3):113-7.

47. Broniscer A, Baker SD, Wetmore C, Pai Panandiker AS, Huang J, Davidoff AM, et al. Phase I trial, pharmacokinetics, and pharmacodynamics of vandetanib and dasatinib in children with newly diagnosed diffuse intrinsic pontine glioma. Clin Cancer Res. 2013;19(11):3050-8.

48. Mount CW, Majzner RG, Sundaresh S, Arnold EP, Kadapakkam M, Haile S, et al. Potent antitumor efficacy of anti-GD2 CAR T cells in H3-K27M(+) diffuse midline gliomas. Nat Med. 2018;24(5):572-9.

49. Gholamin S, Mitra SS, Feroze AH, Liu J, Kahn SA, Zhang M, et al. Disrupting the CD47-SIRPalpha anti-phagocytic axis by a humanized anti-CD47 antibody is an efficacious treatment for malignant pediatric brain tumors. Sci Transl Med. 2017;9(381).

50. Adan A, Kiraz Y, Baran Y. Cell Proliferation and Cytotoxicity Assays. Curr Pharm Biotechnol. 2016;17(14):1213-21.

51. Promega Corporation aaoPGhwpdpc-h-ac-v-a-c-acg-l-c-v-acG. CellTiter-Glo® Luminescent Cell Viability Assay 2021 [

52. Cortes A, Cascante M, Cardenas ML, Cornish-Bowden A. Relationships between inhibition constants, inhibitor concentrations for 50% inhibition and types of inhibition: new ways of analysing data. Biochem J. 2001;357(Pt 1):263-8.

53. Joo M, Park A, Kim K, Son WJ, Lee HS, Lim G, et al. A Deep Learning Model for Cell Growth Inhibition IC50 Prediction and Its Application for Gastric Cancer Patients. Int J Mol Sci. 2019;20(24).

54. Smith MA, Houghton P. A proposal regarding reporting of in vitro testing results. Clin Cancer Res. 2013;19(11):2828-33.

55. Liston DR, Davis M. Clinically Relevant Concentrations of Anticancer Drugs: A Guide for Nonclinical Studies. Clin Cancer Res. 2017;23(14):3489-98.

56. Arrowsmith J, Miller P. Trial watch: phase II and phase III attrition rates 2011-2012. Nat Rev Drug Discov. 2013;12(8):569.

57. Vargo M. Brain tumor rehabilitation. Am J Phys Med Rehabil. 2011;90(5 Suppl 1):S50-62.

58. Aldape K, Brindle KM, Chesler L, Chopra R, Gajjar A, Gilbert MR, et al. Challenges to curing primary brain tumours. Nat Rev Clin Oncol. 2019;16(8):509-20.

59. Chaves C, Decleves X, Taghi M, Menet MC, Lacombe J, Varlet P, et al. Characterization of the Blood-Brain Barrier Integrity and the Brain Transport of SN-38 in an Orthotopic Xenograft Rat Model of Diffuse Intrinsic Pontine Glioma. Pharmaceutics. 2020;12(5).

60. Veringa SJ, Biesmans D, van Vuurden DG, Jansen MH, Wedekind LE, Horsman I, et al. In vitro drug response and efflux transporters associated with drug resistance in pediatric high grade glioma and diffuse intrinsic pontine glioma. PLoS One. 2013;8(4):e61512.

61. Werbrouck C, Evangelista CCS, Lobon-Iglesias MJ, Barret E, Le Teuff G, Merlevede J, et al. TP53 Pathway Alterations Drive Radioresistance in Diffuse Intrinsic Pontine Gliomas (DIPG). Clin Cancer Res. 2019;25(22):6788-800.

62. Mansoori B, Mohammadi A, Davudian S, Shirjang S, Baradaran B. The Different Mechanisms of Cancer Drug Resistance: A Brief Review. Adv Pharm Bull. 2017;7(3):339-48.

63. Lieberman NAP, DeGolier K, Kovar HM, Davis A, Hoglund V, Stevens J, et al. Characterization of the immune microenvironment of diffuse intrinsic pontine glioma: implications for development of immunotherapy. Neuro Oncol. 2019;21(1):83-94.

64. Lin GL, Nagaraja S, Filbin MG, Suva ML, Vogel H, Monje M. Non-inflammatory tumor microenvironment of diffuse intrinsic pontine glioma. Acta Neuropathol Commun. 2018;6(1):51.

65. Boulet MHC, Marsh LK, Howarth A, Woolman A, Farrer NJ. Oxaliplatin and [Pt(R,R-DACH)(panobinostat-2H)] show nanomolar cytotoxicity towards diffuse intrinsic pontine glioma (DIPG). Dalton Trans. 2020;49(17):5703-10.

66. Maintenance of Human Pluripotent Stem Cells in mTeSR Plus. STEMCELL Technologies Inc, Document #10000005507, Version 02. October 2019.

67. Corporation LT. Induction of Neural Stem Cells from Human Pluripotent Stem Cells Using PSC Neural Induction Medium. Publication Number MAN0008031; Revision A0. 30 December 2013.

68. Scientific TF. Differentiating Neural Stem Cells into Neurons and Glial Cells-Protocol. https://wwwthermofishercom/al/en/home/references/protocols/neurobiology/neurobiology-protocols/differentiating-neural-stem-cells-into-neurons-and-glial-cellshtml#3. 17 March 2011.

69. Accelerated maturation and improved functionality of neurons with CultureOne Supplement.

© 2017 Thermo Fisher Scientific Inc. 2017.

70. Trepel J, Mollapour M, Giaccone G, Neckers L. Targeting the dynamic HSP90 complex in cancer. Nat Rev Cancer. 2010;10(8):537-49.

71. Kasibhatla S, Baichwal V, Cai SX, Roth B, Skvortsova I, Skvortsov S, et al. MPC-6827: a small-molecule inhibitor of microtubule formation that is not a substrate for multidrug resistance pumps. Cancer Res. 2007;67(12):5865-71.

72. Eckschlager T, Plch J, Stiborova M, Hrabeta J. Histone Deacetylase Inhibitors as Anticancer Drugs. Int J Mol Sci. 2017;18(7).

73. Kuhn DJ, Chen Q, Voorhees PM, Strader JS, Shenk KD, Sun CM, et al. Potent activity of carfilzomib, a novel, irreversible inhibitor of the ubiquitin-proteasome pathway, against preclinical models of multiple myeloma. Blood. 2007;110(9):3281-90.

74. Zheng S, Zhong Q, Mottamal M, Zhang Q, Zhang C, Lemelle E, et al. Design, synthesis, and biological evaluation of novel pyridine-bridged analogues of combretastatin-A4 as anticancer agents. J Med Chem. 2014;57(8):3369-81.

75. Tu T, Huang J, Lin M, Gao Z, Wu X, Zhang W, et al. CUDC907 reverses pathological phenotype of keloid fibroblasts in vitro and in vivo via dual inhibition of PI3K/Akt/mTOR signaling and HDAC2. Int J Mol Med. 2019;44(5):1789-800.

76. Gehrke I, Bouchard ED, Beiggi S, Poeppl AG, Johnston JB, Gibson SB, et al. On-target effect of FK866, a nicotinamide phosphoribosyl transferase inhibitor, by apoptosis-mediated death in chronic lymphocytic leukemia cells. Clin Cancer Res. 2014;20(18):4861-72.

77. Piva R, Ruggeri B, Williams M, Costa G, Tamagno I, Ferrero D, et al. CEP-18770: A novel, orally active proteasome inhibitor with a tumor-selective pharmacologic profile competitive with bortezomib. Blood. 2008;111(5):2765-75.

78. Parry D, Guzi T, Shanahan F, Davis N, Prabhavalkar D, Wiswell D, et al. Dinaciclib (SCH 727965), a novel and potent cyclin-dependent kinase inhibitor. Mol Cancer Ther. 2010;9(8):2344-53.

79. Heffron TP, Ndubaku CO, Salphati L, Alicke B, Cheong J, Drobnick J, et al. Discovery of Clinical Development Candidate GDC-0084, a Brain Penetrant Inhibitor of PI3K and mTOR. ACS Med Chem Lett. 2016;7(4):351-6.

80. Venkatesan AM, Dehnhardt CM, Delos Santos E, Chen Z, Dos Santos O, Ayral-Kaloustian S, et al. Bis(morpholino-1,3,5-triazine) derivatives: potent adenosine 5'-triphosphate competitive phosphatidylinositol-3-kinase/mammalian target of rapamycin inhibitors: discovery of compound 26 (PKI-587), a highly efficacious dual inhibitor. J Med Chem. 2010;53(6):2636-45.

81. Watson M, Roulston A, Belec L, Billot X, Marcellus R, Bedard D, et al. The small molecule GMX1778 is a potent inhibitor of NAD+ biosynthesis: strategy for enhanced therapy in nicotinic acid phosphoribosyltransferase 1-deficient tumors. Mol Cell Biol. 2009;29(21):5872-88.

82. Chakkath T, Lavergne S, Fan TM, Bunick D, Dirikolu L. Alkylation and Carbamylation Effects of Lomustine and Its Major Metabolites and MGMT Expression in Canine Cells. Vet Sci. 2015;2(2):52-68.

83. Feling RH, Buchanan GO, Mincer TJ, Kauffman CA, Jensen PR, Fenical W. Salinosporamide A: a highly cytotoxic proteasome inhibitor from a novel microbial source, a marine bacterium of the new genus salinospora. Angew Chem Int Ed Engl. 2003;42(3):355-7.

84. Lunn JM, Harris AL. Cytotoxicity of 5-(3-methyl-1-triazeno)imidazole-4-carboxamide (MTIC) on Mer+, Mer+Rem- and Mer- cell lines: differential potentiation by 3-acetamidobenzamide. Br J Cancer. 1988;57(1):54-8.

85. Delmonte A, Sessa C. AVE8062: a new combretastatin derivative vascular disrupting agent. Expert Opin Investig Drugs. 2009;18(10):1541-8.

86. Bonner ER, Waszak SM, Grotzer MA, Mueller S, Nazarian J. Mechanisms of imipridones in targeting mitochondrial metabolism in cancer cells. Neuro Oncol. 2021;23(4):542-56.

87. Chandarlapaty S, Sawai A, Ye Q, Scott A, Silinski M, Huang K, et al. SNX2112, a synthetic heat shock protein 90 inhibitor, has potent antitumor activity against HER kinase-dependent cancers. Clin Cancer Res. 2008;14(1):240-8.

88. Ruegg UT, Burgess GM. Staurosporine, K-252 and UCN-01: potent but nonspecific inhibitors of protein kinases. Trends Pharmacol Sci. 1989;10(6):218-20.

89. Stryckmans PA, Lurie PM, Manaster J, Vamecq G. Mode of action of chemotherapy in vivo on human acute leukemia--II. Vincristine. Eur J Cancer. 1973;9(9):613-20.

90. Gregory RK, Smith IE. Vinorelbine--a clinical review. Br J Cancer. 2000;82(12):1907-13.

91. Holen K, Saltz LB, Hollywood E, Burk K, Hanauske AR. The pharmacokinetics, toxicities, and biologic effects of FK866, a nicotinamide adenine dinucleotide biosynthesis inhibitor. Invest New Drugs. 2008;26(1):45-51.

92. Spreafico A, Delord JP, De Mattos-Arruda L, Berge Y, Rodon J, Cottura E, et al. A first-in-human phase I, dose-escalation, multicentre study of HSP990 administered orally in adult patients with advanced solid malignancies. Br J Cancer. 2015;112(4):650-9.

93. Amengual JE, Lichtenstein R, Lue J, Sawas A, Deng C, Lichtenstein E, et al. A phase 1 study of romidepsin and pralatrexate reveals marked activity in relapsed and refractory T-cell lymphoma. Blood. 2018;131(4):397-407.

94. Clive S, Woo MM, Nydam T, Kelly L, Squier M, Kagan M. Characterizing the disposition, metabolism, and excretion of an orally active pan-deacetylase inhibitor, panobinostat, via trace

radiolabeled 14C material in advanced cancer patients. Cancer Chemother Pharmacol. 2012;70(4):513-22.

95. Harrison SJ, Mainwaring P, Price T, Millward MJ, Padrik P, Underhill CR, et al. Phase I Clinical Trial of Marizomib (NPI-0052) in Patients with Advanced Malignancies Including Multiple Myeloma: Study NPI-0052-102 Final Results. Clin Cancer Res. 2016;22(18):4559-66.

96. Kortmansky J, Shah MA, Kaubisch A, Weyerbacher A, Yi S, Tong W, et al. Phase I trial of the cyclin-dependent kinase inhibitor and protein kinase C inhibitor 7-hydroxystaurosporine in combination with Fluorouracil in patients with advanced solid tumors. J Clin Oncol. 2005;23(9):1875-84.

97. Yang F, Jiang M, Lu M, Hu P, Wang H, Jiang J. Pharmacokinetic Behavior of Vincristine and Safety Following Intravenous Administration of Vincristine Sulfate Liposome Injection in Chinese Patients With Malignant Lymphoma. Front Pharmacol. 2018;9:991.

98. Wu G, Wu L, Zhou H, Lin M, Peng L, Wang Y, et al. A Phase I Comparative Pharmacokinetic and Safety Study of Two Intravenous Formulations of Vinorelbine in Patients With Advanced Non-Small Cell Lung Cancer. Front Pharmacol. 2019;10:774.

99. Kastrissios H, Chao NJ, Blaschke TF. Pharmacokinetics of high-dose oral CCNU in bone marrow transplant patients. Cancer Chemother Pharmacol. 1996;38(5):425-30.

100. Tsimberidou AM, Akerley W, Schabel MC, Hong DS, Uehara C, Chhabra A, et al. Phase I clinical trial of MPC-6827 (Azixa), a microtubule destabilizing agent, in patients with advanced cancer. Mol Cancer Ther. 2010;9(12):3410-9.

101. Hovstadius P, Larsson R, Jonsson E, Skov T, Kissmeyer AM, Krasilnikoff K, et al. A Phase I study of CHS 828 in patients with solid tumor malignancy. Clin Cancer Res. 2002;8(9):2843-50.

102. Venugopal B, Baird R, Kristeleit RS, Plummer R, Cowan R, Stewart A, et al. A phase I study of quisinostat (JNJ-26481585), an oral hydroxamate histone deacetylase inhibitor with evidence of target modulation and antitumor activity, in patients with advanced solid tumors. Clin Cancer Res. 2013;19(15):4262-72.

103. Nowakowski GS, McCollum AK, Ames MM, Mandrekar SJ, Reid JM, Adjei AA, et al. A phase I trial of twice-weekly 17-allylamino-demethoxy-geldanamycin in patients with advanced cancer. Clin Cancer Res. 2006;12(20 Pt 1):6087-93.

104. Younes A, Berdeja JG, Patel MR, Flinn I, Gerecitano JF, Neelapu SS, et al. Safety, tolerability, and preliminary activity of CUDC-907, a first-in-class, oral, dual inhibitor of HDAC and PI3K, in patients with relapsed or refractory lymphoma or multiple myeloma: an open-label, dose-escalation, phase 1 trial. Lancet Oncol. 2016;17(5):622-31.

105. Gallerani E, Zucchetti M, Brunelli D, Marangon E, Noberasco C, Hess D, et al. A first in human phase I study of the proteasome inhibitor CEP-18770 in patients with advanced solid tumours and multiple myeloma. Eur J Cancer. 2013;49(2):290-6.

106. Sessa C, Shapiro GI, Bhalla KN, Britten C, Jacks KS, Mita M, et al. First-in-human phase I dose-escalation study of the HSP90 inhibitor AUY922 in patients with advanced solid tumors. Clin Cancer Res. 2013;19(13):3671-80.

107. Eskens FA, Tresca P, Tosi D, Van Doorn L, Fontaine H, Van der Gaast A, et al. A phase I pharmacokinetic study of the vascular disrupting agent ombrabulin (AVE8062) and docetaxel in advanced solid tumours. Br J Cancer. 2014;110(9):2170-7.

108. Quach H, White D, Spencer A, Ho PJ, Bhutani D, White M, et al. Pharmacokinetics and safety of carfilzomib in patients with relapsed multiple myeloma and end-stage renal disease (ESRD): an open-label, single-arm, phase I study. Cancer Chemother Pharmacol. 2017;79(6):1067-76.

109. Infante JR, Weiss GJ, Jones S, Tibes R, Bauer TM, Bendell JC, et al. Phase I dose-escalation studies of SNX-5422, an orally bioavailable heat shock protein 90 inhibitor, in patients with refractory solid tumours. Eur J Cancer. 2014;50(17):2897-904.

110. Shapiro GI, Kwak E, Dezube BJ, Yule M, Ayrton J, Lyons J, et al. First-in-human phase I dose escalation study of a second-generation non-ansamycin HSP90 inhibitor, AT13387, in patients with advanced solid tumors. Clin Cancer Res. 2015;21(1):87-97.

111. Mita MM, Mita AC, Moseley JL, Poon J, Small KA, Jou YM, et al. Phase 1 safety, pharmacokinetic and pharmacodynamic study of the cyclin-dependent kinase inhibitor dinaciclib administered every three weeks in patients with advanced malignancies. Br J Cancer. 2017;117(9):1258-68.

112. Takebe N, Beumer JH, Kummar S, Kiesel BF, Dowlati A, O'Sullivan Coyne G, et al. A phase I pharmacokinetic study of belinostat in patients with advanced cancers and varying degrees of liver dysfunction. Br J Clin Pharmacol. 2019;85(11):2499-511.

113. Rubin EH, Agrawal NG, Friedman EJ, Scott P, Mazina KE, Sun L, et al. A study to determine the effects of food and multiple dosing on the pharmacokinetics of vorinostat given orally to patients with advanced cancer. Clin Cancer Res. 2006;12(23):7039-45.

114. Houk BE, Alvey CW, Visswanathan R, Kirkovsky L, Matschke KT, Kimoto E, et al. Distribution, Metabolism, and Excretion of Gedatolisib in Healthy Male Volunteers After a Single Intravenous Infusion. Clin Pharmacol Drug Dev. 2019;8(1):22-31.

115. Pili R, Salumbides B, Zhao M, Altiok S, Qian D, Zwiebel J, et al. Phase I study of the histone deacetylase inhibitor entinostat in combination with 13-cis retinoic acid in patients with solid tumours. Br J Cancer. 2012;106(1):77-84.

116. Diez BD, Statkevich P, Zhu Y, Abutarif MA, Xuan F, Kantesaria B, et al. Evaluation of the exposure equivalence of oral versus intravenous temozolomide. Cancer Chemother Pharmacol. 2010;65(4):727-34.

117. He X, Li S, Huang H, Li Z, Chen L, Ye S, et al. A pharmacokinetic and safety study of single dose intravenous combretastatin A4 phosphate in Chinese patients with refractory solid tumours. Br J Clin Pharmacol. 2011;71(6):860-70.

118. Wen PY, Cloughesy TF, Olivero AG, Morrissey KM, Wilson TR, Lu X, et al. First-in-Human Phase I Study to Evaluate the Brain-Penetrant PI3K/mTOR Inhibitor GDC-0084 in Patients with Progressive or Recurrent High-Grade Glioma. Clin Cancer Res. 2020;26(8):1820-8.

119. Stein MN, Malhotra J, Tarapore RS, Malhotra U, Silk AW, Chan N, et al. Safety and enhanced immunostimulatory activity of the DRD2 antagonist ONC201 in advanced solid tumor patients with weekly oral administration. J Immunother Cancer. 2019;7(1):136.

120. Gunhanlar N, Shpak G, van der Kroeg M, Gouty-Colomer LA, Munshi ST, Lendemeijer B, et al. A simplified protocol for differentiation of electrophysiologically mature neuronal networks from human induced pluripotent stem cells. Mol Psychiatry. 2018;23(5):1336-44.

121. Krug AK, Balmer NV, Matt F, Schonenberger F, Merhof D, Leist M. Evaluation of a human neurite growth assay as specific screen for developmental neurotoxicants. Arch Toxicol. 2013;87(12):2215-31.

122. Radio NM, Mundy WR. Developmental neurotoxicity testing in vitro: models for assessing chemical effects on neurite outgrowth. Neurotoxicology. 2008;29(3):361-76.

123. Filous AR, Silver J. Neurite Outgrowth Assay. Bio Protoc. 2016;6(1).

124. Dehmelt L, Poplawski G, Hwang E, Halpain S. NeuriteQuant: an open source toolkit for high content screens of neuronal morphogenesis. BMC Neurosci. 2011;12:100.

125. Stone JB, DeAngelis LM. Cancer-treatment-induced neurotoxicity--focus on newer treatments. Nat Rev Clin Oncol. 2016;13(2):92-105.

126. Legha SS. Vincristine neurotoxicity. Pathophysiology and management. Med Toxicol. 1986;1(6):421-7.

127. Warren KE. Diffuse intrinsic pontine glioma: poised for progress. Front Oncol. 2012;2:205.

128. Gomis-Tena J, Brown BM, Cano J, Trenor B, Yang PC, Saiz J, et al. When Does the IC50 Accurately Assess the Blocking Potency of a Drug? J Chem Inf Model. 2020;60(3):1779-90.

129. Motl S, Zhuang Y, Waters CM, Stewart CF. Pharmacokinetic considerations in the treatment of CNS tumours. Clin Pharmacokinet. 2006;45(9):871-903.

130. Tukker AM, de Groot MW, Wijnolts FM, Kasteel EE, Hondebrink L, Westerink RH. Is the time right for in vitro neurotoxicity testing using human iPSC-derived neurons? ALTEX. 2016;33(3):261-71.